Luiz Felipe Klöppel

DESENVOLVIMENTO DE UM SISTEMA DE MONITORAMENTO BASEADO EM FOTODETETOR PARA A ABLAÇÃO A LASER DE FILMES METÁLICOS SOBRE SUBSTRATOS POLIMÉRICOS

Dissertação submetida ao Programa de Pós-Graduação em Engenharia Mecânica da Universidade Federal de Santa Catarina para a obtenção do Grau de Mestre em Engenharia Mecânica.
Orientador: Prof. Walter Lindolfo Weingaertner, Dr.-Ing.
Coorientador: Dipl.-Ing. (FH) B.Eng. (hon) Ulrich Thombansen, M.Sc.

Florianópolis
2015

Ficha de identificação da obra elaborada pelo autor,
através do Programa de Geração Automática da Biblioteca Universitária da UFSC.

Klöppel, Luiz Felipe
Desenvolvimento de um sistema de monitoramento baseado em fotodetetor para a ablação a laser de filmes metálicos sobre substratos poliméricos / Luiz Felipe Klöppel ; orientador, Walter Lindolfo Weingaertner ; coorientador, Ulrich Thombansen. - Florianópolis, SC, 2015.
118 p.

Dissertação (mestrado) - Universidade Federal de Santa Catarina, Centro Tecnológico. Programa de Pós-Graduação em Engenharia Mecânica.

Inclui referências

1. Engenharia Mecânica. 2. Monitoramento de processo. 3. Ablação a laser. 4. Análise do espectro ótico. 5. Fotodetetores. I. Weingaertner, Walter Lindolfo. II. Thombansen, Ulrich. III. Universidade Federal de Santa Catarina. Programa de Pós-Graduação em Engenharia Mecânica. IV. Título.

Luiz Felipe Klöppel

DEVELOPMENT OF A PHOTODETECTOR-BASED MONITORING SYSTEM FOR LASER ABLATION OF METAL LAYERS ON POLYMERIC SUBSTRATE

Dissertação submetida ao Programa de Pós-Graduação em Engenharia Mecânica da Universidade Federal de Santa Catarina para a obtenção do Grau de Mestre em Engenharia Mecânica.
Orientador: Prof. Walter Lindolfo Weingaertner, Dr.-Ing.
Coorientador: Dipl.-Ing. (FH) B.Eng. (hon) Ulrich Thombansen, M.Sc.

Florianópolis
2015

Luiz Felipe Klöppel

DESENVOLVIMENTO DE UM SISTEMA DE MONITORAMENTO BASEADO EM FOTODETETOR PARA A ABLAÇÃO A LASER DE FILMES METÁLICOS SOBRE SUBSTRATOS POLIMÉRICOS

Esta Dissertação foi julgada adequada para obtenção do Título de "Mestre em Engenharia Mecânica", e aprovada em sua forma final pelo Programa de Pós-Graduação em Engenharia Mecânica.

Florianópolis, 27 de Fevereiro de 2015.

____
Prof. Armando Albertazzi G. Junior, Dr.Eng.
Coordenador do Curso

Banca Examinadora:

____
Prof. Walter Lindolfo Weingaertner, Dr.-Ing.
Orientador
Universidade Federal de Santa Catarina

____
Prof. Armando Albertazzi G. Junior, Dr.
Universidade Federal de Santa Catarina

____
Prof. Milton Pereira, Dr.Eng.
Instituto Federal de Santa Catarina

____
Prof. Rolf Bertrand Schroeter, Dr.Eng.
Universidade Federal de Santa Catarina

To my family, for all the love and support.

AKNOWLEDGEMENTS

I am thankful to all those who somehow contributed to the development of this work, especially:

To Prof. Dr. –Ing. Walter Lindolfo Weingaertner for the advices, support and lessons given since my first academic years;

To M. Sc. Dipl. –Ing. (FH) B. Eng. (hon) Ulrich Thombansen for the guidance and assistance during my time at Fraunhofer Institute for Laser Technology ILT, particularly in the planning and performance of the activities of this work;

To my colleagues from Fraunhofer ILT for the nice moments inside and outside work, making my experience abroad unforgettable. A special thanks to those who participated directly or indirectly in Project MaLDeAN;

To my colleagues from Precision Engineering Laboratory – LMP for sharing their motivation and willingness to know new things;

To my family for the love, support and for teaching me my values;

To my friends in Brazil and abroad for all the good moments together, making things easier and more pleasant.

RESUMO

O advento dos lasers de pulsos ultracurtos (USP, sigla em inglês para *ultrashort pulse*) permitiram novas possibilidades na fabricação em micro e nanoescala. Características destes lasers, como alta resolução lateral devido a capacidade de ser precisamente focado em alguns micrometros, baixo calor fornecido à peça e alta flexibilidade são os principais atributos desta ferramenta em processos para estruturação e funcionalização de superfícies. Apesar das vantagens dos lasers de pulsos ultracurtos, suas aplicações são relativamente novas e necessitam desenvolvimento. Demandas crescentes em qualidade e produtividade em ablação a laser criam a necessidade de aplicar sistemas de monitoramento de processos na produção industrial. No campo dos eletrônicos, especialmente, a atual miniaturização dos produtos requer pequenos componentes de alta precisão. A fabricação de placas de circuito impresso por laser requer uma ablação precisa de filmes finos de cobre sobre substrato polimérico, com mínimo dano ao substrato. Com o objetivo de aumentar a confiabilidade do processo para uma completa ablação de cobre, um sistema de monitoramento de alta velocidade, com resolução espacial, baseado em analisadores de espectro óptico com grade de difração é desenvolvido e integrado à máquina de ablação a laser. Na ablação a laser de placas de circuito impresso, a camada de cobre é removida em determinadas regiões pela interação do feixe laser com a peça. Esta interação emite radiação em comprimentos de ondas específicos, de acordo com o material. Para monitorar o processo, o espectro da radiação emitida é observado. Quando o espectro muda para um padrão diferente de comprimentos de onda, considera-se que a camada de cobre foi removida e a camada de polímero interage com o laser. Um sistema óptico capaz de separar o espectro da radiação emitida é montado. Para cumprir as exigências do processo e detectar a emissão, um fotodetector de alta velocidade e alta sensibilidade é utilizado. Informações de posição do sistema de deflexão do feixe (*scanner*) são incorporadas às informações de emissão do fotodetector e um mapa de emissão é construído. O sistema de monitoramento é capaz de observar a radiação emitida por diferentes materiais. Regiões onde o cobre está presente podem ser bem identificadas. O mapa de emissão se apresenta como um estratégia válida para o monitoramento do processo de ablação a laser.

Palavras-chave: ablação a laser, monitoramento de processo, analisador de espectro óptico, fotodetector, mapa de emissão.

ABSTRACT

The advent of ultrashort pulse (USP) lasers allowed new possibilities in micro and nanoscale manufacturing. Characteristics of USP lasers, like high lateral resolution due to precise focusability down to a few micrometers, low heat input and high flexibility are main features of laser tools and processes for precision structuring and surface functionalization. Despite the advantages of USP lasers, its applications are relatively new and need further development. Increasing demand on quality and productivity in laser ablation creates the necessity to apply process monitoring systems in industrial manufacturing. In the field of electronics, especially, the ongoing miniaturization of products requires small components with high accuracy. The manufacturing of printed circuit boards (PCBs) by laser demands a precise ablation of thin copper layer on polymeric substrate, with small substrate damage. Aiming to increase the process reliability for a complete ablation of copper, a fast spatially resolved process monitoring system based on diffraction grating optical spectrum analyzers is developed and integrated to the laser ablation machine. In the laser ablation of printed circuit boards, unwanted copper layer is removed by the interaction of the laser beam with the material. This interaction emits radiation in specific wavelengths, according to the material. To monitor the process, the spectrum of the emitted radiation is observed. When the spectrum changes for a different wavelengths pattern, it is considered that the copper layer was completely removed and the polymer layer is interacting with the laser. An optical system able to separate the emitted radiation spectrum is assembled. To fulfill the requirements of the process and to detect the emitted radiation, a high speed and high sensitive photodetector is applied. Position information from the beam deflecting system (scanner) is implemented to the emission information from the photodetector and an emission map is built. The monitoring system based on photodetector is able to detect radiation emitted by different materials. Regions where copper is present can be well identified. The emission map shows to be a valid strategy for laser ablation process monitoring.

Keywords: laser ablation, process monitoring, optical spectrum analyzer, photodetector, emission map.

RESUMO EXPANDIDO

Introdução

O advento dos lasers de pulsos ultracurtos (USP, sigla em inglês para *ultrashort pulse*) permitiram novas possibilidades na fabricação em micro e nanoescala. Características destes lasers, como alta resolução lateral devido a capacidade de serem precisamente focados em alguns micrometros, baixo calor fornecido à peça e alta flexibilidade são os principais atributos desta ferramenta em processos para estruturação e funcionalização de superfícies.

Apesar das vantagens dos lasers de pulsos ultracurtos, suas aplicações são relativamente novas e necessitam desenvolvimento. Demandas crescentes em qualidade e produtividade em ablação a laser criam a necessidade de aplicar sistemas de monitoramento de processos na produção industrial. No campo dos eletrônicos, especialmente, a atual miniaturização dos produtos requer pequenos componentes de alta precisão e circuitos com alta densidade de interconexões.

Objetivo

A fabricação de placas de circuito impresso por laser exige uma ablação precisa de filmes finos de cobre sobre substrato polimérico, com mínimo dano ao substrato. Neste trabalho um protótipo de sistema de monitoramento coaxial de alta velocidade, com resolução espacial é desenvolvido e descrito. O protótipo tem por objetivo aumentar a confiabilidade do processo para uma completa ablação do filme de cobre para a formação de trilhas condutoras.

Metodologia

A configuração coaxial é utilizada uma vez que nela o sensor sempre obtém informações da zona de interação entre laser e peça, independentemente dos movimentos do scanner sobre o campo de trabalho.

Como estratégia de monitoramento, utiliza-se a análise do espectro da radiação emitida durante o processo. Na ablação a laser de placas de circuito impresso, a camada de cobre é removida em determinadas regiões pela interação do feixe laser com a peça. Esta interação emite radiação em comprimentos de ondas específicos, de acordo com o material da peça. Com o monitoramento, observa-se o

padrão espectral da radiação emitida. Quando este espectro muda para um padrão diferente de comprimentos de onda, considera-se que a camada de cobre foi removida e a camada de polímero interage com o laser.

Um sistema óptico capaz de separar o espectro da radiação emitida é montado. O sistema se baseia em analisadores de espectro óptico com grade de difração, disposto na configuração do monocromador de Czerny-Turner. A integração com a máquina de ablação a laser é feita através da utilização de um espelho dicroico, capaz de refletir os comprimentos de onda do laser de trabalho e transmitir os comprimentos de onda emitidos pelo processamento do cobre. A Figura 1 (esq.) mostra o conceito do sistema de monitoramento integrado à máquina de ablação. A Figura 1 (dir.) apresenta o arranjo óptico do protótipo do sistema de monitoramento.

Figura 1 – Esq.: Conceito do sistema de monitoramento. Dir.: Arranjo óptico do protótipo.

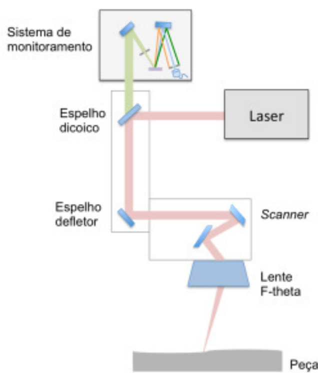

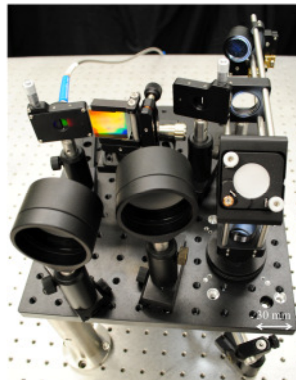

Fonte: O autor.

Para cumprir as exigências do processo e detectar a emissão, um fotodetector de alta velocidade e alta sensibilidade é utilizado. Para tal utiliza-se um fotomultiplicador de silício, que além de unir as características necessárias de velocidade e sensibilidade, é relativamente robusto, ideal para aplicações industriais. Através de uma função da placa de controle do scanner, que permite ler a posição atual do feixe sobre a peça, as coordenadas [x(t), y(t)] do sistema de deflexão do feixe (*scanner*) são incorporadas às informações de emissão do fotodetector

por meio de um circuito integrado FPGA (*free programmable gate array*). A integração das 3 coordenadas possibilita a construção de um mapa de emissão da radiação ao longo da peça.

Resultados

Testes durante o processamento de placas de circuito impresso demonstram a capacidade do protótipo em identificar o sinal emitido pelo recobrimento de cobre e, assim, distinguir o cobre de outros materiais. A Figura 2 mostra o progresso do processo de ablação a laser de placas de circuito impresso entre as camadas 16 e 24. O recobrimento de cobre, caracterizado em verde, começa a desaparecer a partir da camada 23 e é praticamente removido na camada 24, restando apenas o substrato, caracterizado em azul.

Figura 2 - Progresso do processo de remoção ao longo de 9 camadas.

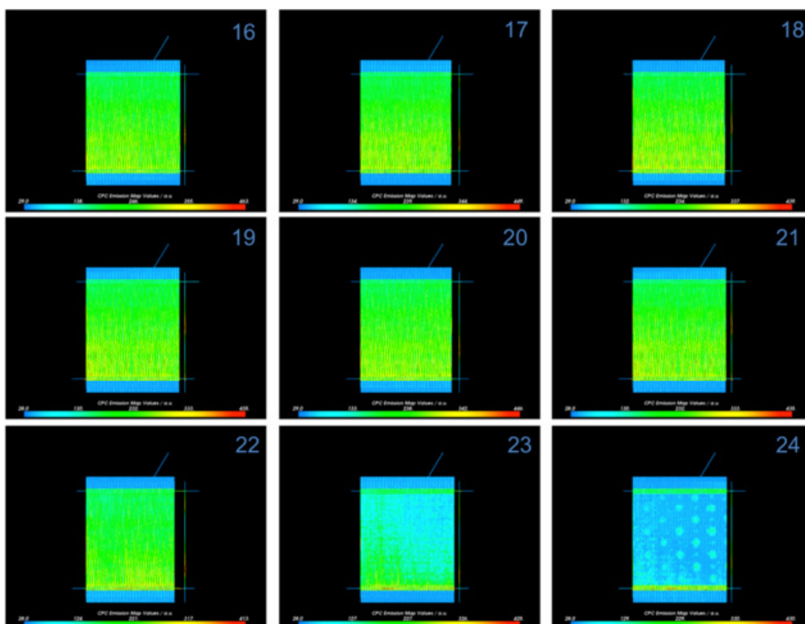

Fonte: O autor.

Desta forma, o sistema de monitoramento é capaz de observar a radiação emitida por diferentes materiais. Regiões onde o cobre está

presente podem ser bem identificadas. O mapa de emissão se apresenta como um estratégia válida para o monitoramento do processo de ablação a laser.

LIST OF FIGURES

Figure 1 - Properties of light from a flashlight (1) and from a laser light (2). ...31
Figure 2 – a) Intensity distribution and shape of a Gaussian laser beam. b) Various mode patterns. ...32
Figure 3 – Partial classification of manufacturing processes according to DIN 8580 and DIN 8590. Some subgroups are hidden to facilitate understanding. ..34
Figure 4 - Interaction between laser ablation mechanisms. ...35
Figure 5 - Basic principle of laser ablation. ...36
Figure 6 - Laser ablation with mask (a) and scanner (b). ...37
Figure 7 – Laser ablation process scheme: a) single pulse; b) track; c) area. ...37
Figure 8 - Influence of the pulse width in laser ablation of steel foil. For laser pulses at 780 nm: a) τ_l = 200 fs, F = 0,5 J/cm^2; b) τ_l = 80 ps, F = 3,7 J/cm^2; c) τ_l = 3,3 ns, F = 4,2 J/cm^2. ...40
Figure 9 - Relationship between beam intensity and ablated diameter. ...41
Figure 10 - a) Free form ablation of thin films. b) Flexible multicolor OLED on foil of stainless steel. c) Shaped holes produced by 5-axis-trepanning. d) Laser cutted stent from stainless steel with details geometries < 100 µm. ...44
Figure 11 - a) Super hydrophobic surface microstructured with picosecond laser. b) Laser structuring of cylinder for improvement of tribological characteristics. c) Nanostructured hot-embossing roll made of heat-treated steel. d) Mold textured by laser ablation. e) Light guiding structure made of micro lenses for a uniform light distribution. ...45
Figure 12 - a) Microvia in resin coated copper D = 75 µm. b) Laser cut flexible printed board. c) Magnified HDI circuit area patterned by LDI. d) 50 µm tracks/gaps on Cu base material. ...49
Figure 13 - a) Laser structured PCB sample. b) ProtoLaser U3 processing unit. ...50
Figure 14 - Lateral (left) and coaxial (right) arrangement for laser process monitoring. ...52
Figure 15 - Scheme of Spectral Domain OCT (SD-OCT). FC means fiber coupler and CCD means charged-coupled device. ...54
Figure 16 - Basic set-up for laser-induced breakdown spectrometry. ...55
Figure 17 - Fabry-Pérot interferometer-based optical spectrum analyzer. ...56
Figure 18 - Michelson interferometer-based optical spectrum analyzer. ...57
Figure 19 – Simplified scheme of a diffraction grating-based optical spectrum analyzer. ...58
Figure 20 - Diffraction of light at a diffraction grating. ...60
Figure 21 – Output beams of diffraction orders. ...61
Figure 22 - Czerny-Turner configuration. ...62
Figure 23 - Ebert-Fastie configuration. ...63
Figure 24 - Rowland Circle configuration. ...63
Figure 25 - Offner configuration. ...64
Figure 26 - LASERTEC 50 (LT 50) machine platform. ...68
Figure 27 - Methodology for the development of the monitoring system. ...70

Figure 28 - Concept of the monitoring system. 74
Figure 29 - Copper emission spectrum for spectrometer integration times of 1 s, 2 s and 3 s, during laser processing. Dark spectrum is subtracted. 75
Figure 30 – Comparison of copper and FR-4 emission spectrum for 1 s integration time. Dark spectrum is subtracted. 76
Figure 31 - SensL Mini SL photon detection efficiency..................................78
Figure 32 - Detail of the optical layout...79
Figure 33 - Prototype assembly. 83
Figure 34 - Transmission measurements of Rodenstock (red line) and Sill color-corrected (blue line) f-theta lenses. Both curves are normalized to their maximum values...84
Figure 35 - Spectral analysis of the deflecting mirror. 85
Figure 36 – Spectral analysis of the dichroic mirror...86
Figure 37 - Adaptations on the breadboard for mechanical integration............87
Figure 38 - RTC5 control interface. 88
Figure 39 - Block diagram of the data analysis system. 89
Figure 40 - Pen-ray line source..91
Figure 41 - Determination of the system resolution. 92
Figure 42 - Image of part of the neon pen-ray LSP032 line source spectrum. ..92
Figure 43 - Alignment of the optical components. 93
Figure 44 - Prototype calibration..94
Figure 45 - Monitoring system assembled in the machine. 95
Figure 46 - Prototype isolated in a matte black aluminum box. 95
Figure 47 - Recognition of copper tracks. P = 12,5 W; V_s = 2 m/s. 96
Figure 48 - Progress of ablated layers. P = 12,5 W; V_s = 2 m/s. 97
Figure 49 – Comparison of microscope picture detail and emission map. 98
Figure 50 - Details recognition and mirror drift. Layer 24; P = 12,5 W; V_s = 2 m/s. 99
Figure 51 - Low accuracy of scanner in high speeds. Layer 47; P = 12,5 W; V_s = 4 m/s 100
Figure 52 - Optical layout simulated with the software Zemax......................115
Figure 53 – Progress of laser ablation process. P = 12,5 W; V_s = 2 m/s. 116
Figure 54 - Sensl 30035 performance parameters. 117
Figure 55 – Diffraction grating typical efficiency – 830 g/mm. 118

LIST OF TABLES

Table 1 - Comparison of different removal processes. 42
Table 2 - Laser source characteristics. 68
Table 3 - Process parameters. 69
Table 4 - Comparison of various detector technologies.....................................77
Table 5 - Optical components specifications. 81

LIST OF ABBREVIATIONS

AD	analog-digital
APD	avalanche photodiode
CAD	computer-aided design
CCD	charged-coupled device
CPC	coaxial process control
cw	continuous wave
EDM	Electrical discharge machining
FC	fiber coupler
FD-OCT	Fourier domain optical coherence tomography
FPGA	field-programmable gate array
FR	flame retardant
FWHM	Full width at half-maximum
HAZ	heat affected zone
HDI	high density interconnect
HR	high reflective
ILT	Institute for Laser Technology
LDI	laser direct imaging
LDS	laser direct structuring
LIBS	laser-induced breakdown spectrometry
LIESA	laser-induced emission spectral analysis
LIPS	laser induced plasma spectrometry
LMP	Precision Engineering Laboratory
MID	molded interconnect device
MSM	metal-semiconductor-metal
NIR	near infrared
OCT	optical coherence tomography
OD	optical density
OLED	organic light emitting diode
PCB	printed circuit board
PDA	photodiode array
PDE	photon detection efficiency
PI	polyimid
PMT	photomultiplier tube

PTFE	polytetrafluoroethylene
R	reflection
RAL	reflective aluminum coating
SD-OCT	spectral domain optical coherence tomography
SPM	silicon photomultiplier
SS-OCT	swept source optical coherence tomography
TEM	transverse electromagnetic mode
UFSC	Federal University of Santa Catarina
UV	ultraviolet

LIST OF SYMBOLS

Symbol	Description
α	absorption coefficient (p.36)
α	angle of incidence (p. 57)
β	angle of diffraction (for the diffraction grating)
γ	blaze angle
Θ	beam divergence angle
λ	wavelength
τ_l	pulse width
ϕ; F	fluence
D	ablated diameter
d	distance between adjacent grooves
d_w	working spot diameter
f	focal length
f_{rep}	pulse repetition rate
h	ablation depth
I	intensity
I_0	intensity for $r = 0$
I_{th}	threshold intensity
L	length of focus
l_α	absorption length
m	diffraction order
P	average laser output power
P_{peak}	peak power
r	distance from the center of the beam
tH	pulse length
t_p	pulse period
Vs	scan speed
w_0 ; w_e	radius of the laser focus
$2w_0$	beam waist
z_R	Rayleigh length

CONTENTS

1 INTRODUCTION **29**
1.1 OBJECTIVES 30
1.1.1 Aim **30**
1.1.2 Objectives **30**
2 LITERATURE REVIEW **31**
2.1 LASER BEAM CHARACTERISTICS 31
2.1.1 Wavelength **31**
2.1.2 Coherence **31**
2.1.3 Transverse Mode and Beam Radius **32**
2.1.4 Operating Mode **33**
2.2 LASER ABLATION 33
2.2.1 Definition and Working Principle **35**
2.2.2 Theoretical Background **38**
2.2.3 Applications **41**
2.3 Laser Ablation in Printed Circuit Boards 45
2.4 PROCESS MONITORING 50
2.4.1 Process Monitoring in Laser Ablation **53**
2.5 OPTICAL SPECTRUM ANALYSIS 55
2.5.1 Interferometer-based Optical Spectrum Analyzers **56**
2.5.2 Diffraction Grating-based Optical Spectrum Analyzers . **58**
2.5.3 Photodetectors **64**
3 METHODOLOGY **67**
3.1 EQUIPMENT AND MATERIALS 67
3.1.1 Laser Ablation Machine **67**
3.1.2 Laser Source **68**
3.1.3 Optical Spectrum Analyzers **68**
3.1.4 Material **69**
3.2 PROTOTYPE DEVELOPMENT 69
4 CONCEPT OF THE SENSOR SYSTEM **73**
4.1 DEFINITION OF THE CONCEPT 73
4.2 OPTICAL SIMULATION 78
5 IMPLEMENTATION OF THE SENSOR SYSTEM **81**
5.1 CHARACTERIZATION OF THE OPTICAL COMPONENTS 81
5.1.1 Monitoring System Components and Assembly **81**
5.1.2 LT 50 Components **83**
5.2 MACHINE INTEGRATION 86
5.2.1 Mechanical Integration **86**
5.2.2 Control Interface **87**

6 CALIBRATION AND VERIFICATION 91
6.1 RESOLUTION AND CALIBRATION OF THE SYSTEM........91
6.2 VERIFICATION...94
7 CONCLUSION 101
7.1 SUGGESTIONS FOR FUTURE WORK 102
REFERENCES..103
APPENDIX A – Monitoring system optical layout..........................115
APPENDIX B – Progress of laser ablation process 116
ATTACHMENT A – Sensl performance parameters 117
ATTACHMENT B – Diffraction grating typical efficiency...........118

INTRODUCTION

Laser ablation with ultrashort pulses offers various advantages regarding quality and accuracy of the processed part. It has opened new possibilities in micromachining, becoming suitable for various industrial applications. Surface functionalization and innovative part designs made by laser ablation are found in different areas, such as aerospace, automotive, medical and electronics industry, just to name a few. However, short pulse lasers are still in the industrial use at the beginning of development. They are usually expensive and in some circumstances, even with modern equipment, they do not fit concretely to the applications. In these cases time and resources are consumed by performing trials to determine appropriate strategies that guarantee a high quality level of the produced part.

In the occasions where the definition of stable parameters is not possible, process monitoring becomes an important tool to assure the quality designed for the process and for the product. Online monitoring permits fast reactions in the case of quality decrease in the process, saving efforts and resources avoiding the production of a non-conforming part. The predominant process monitoring approaches in laser ablation are associated to the use of optical spectrum analyzers, either in optical coherence tomography or in spectroscopic analysis.

Ultrashort pulse laser ablation involves high speed movements of the beam into the working field. The application of commercial spectrometers for analyzing the radiation emitted during the process comes to be a challenge, since most of them are unable to reach short enough response times required by the process. Moreover, processing materials with ultrashort pulses, on one hand it is possible to remove in each layer precise small amounts of material, with practically no damage to the substrate. On the other hand, since less volume of material is ablated per pulse, the intensity of the radiation emitted from the process is relatively low for the sensitivity of most commercial spectrometers.

In the scope of the joint project MaLDeAN of the Fraunhofer Institute for Laser Technology ILT and the companies Limo Lissotschenko Mikrooptik and LPKF Laser & Electronics, a precision laser ablation process of thin metal layers on polymeric substrate is developed. The process enables the flexible and also micro-scale manufacturing of conducting structures in printed circuit boards. The objective of Fraunhofer ILT, beyond determining process parameters, is to develop a spatially and temporally resolved process monitoring

solution. The development of the monitoring solution based on a high speed and high sensitive optical spectrum analyzer as well as its findings are described in this work.

The elaboration of this master project at the Fraunhofer Institute for Laser Technology was possible due to the cooperation between the German research institute and the Precision Engineering Laboratory – LMP from the Federal University of Santa Catarina – UFSC.

1.1 OBJECTIVES

1.1.1 Aim

The work aims to develop a temporally and spatially resolved monitoring system based on the analysis of the process emission in laser ablation of metal layers on polymeric substrate.

1.1.2 Objectives

- Understand the principle of operation of optical spectrum analyzers;
- Define a concept for the monitoring system;
- Create a monitoring system prototype for the laser ablation process;
- Analyze and adequate the optical and mechanical components of the laser ablation machine for the integration of the monitoring system;
- Evaluate the performance of the monitoring system in the laser ablation of printed circuit boards by recognizing the presence of copper layer on substrate.

2 LITERATURE REVIEW

2.1 LASER BEAM CHARACTERISTICS

Lasers are optical devices introduced in 1960 that use the phenomenon of stimulated emission identified by Albert Einstein to produce highly directional, high-intensity light [1, 2]. Laser beams are rays of electromagnetic radiation with particular properties of wavelength, coherence, power distribution and beam diameter [3].

2.1.1 Wavelength

Radiation from a laser is amongst the purist spectral forms of radiation available. It is considered monochromatic, i.e. it is pure in color (wavelength or frequency) or, in other words, it has a narrow frequency bandwidth. The wavelength depends on transitions taking place by stimulated emission. The narrowing is enhanced with highly reflecting mirrors, stable cavity components and providing temperature stability [1, 3].

2.1.2 Coherence

Laser light is coherent. The various portions of light are in phase, or in step with each other, producing a continuous laser beam [4]. Figure 1 illustrates a comparison of incandescent bulb light with laser light. Besides coherence, it is also possible to notice the monochromatic property of the laser beam.

Figure 1 - Properties of light from a flashlight (1) and from a laser light (2).

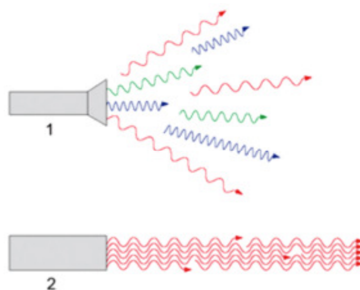

Source: [4].

2.1.3 Transverse Mode and Beam Radius

Laser beams can have different spatial power density distribution, also known as intensity distributions. It describes the power density across the beam cross-section. The numbers of power density distribution are called transverse electromagnetic modes – TEM. The fundamental distribution for a circular beam is the Gaussian distribution (TEM 00) [4]. Figure 2-a exhibits the intensity distribution and shape of a Gaussian laser beam near the focal plane. $2w_0$ is the beam waist; $L = 2z_R$ the length (depth) of the focus, where z_R is the Rayleigh length; and Θ the beam divergence angle (for some authors the angle displayed in Figure 2-a is the divergence half-angle). Dotted curves indicate the shape of the wave front. Figure 2-b shows several mode patterns.

Figure 2 – a) Intensity distribution and shape of a Gaussian laser beam. b) Various mode patterns.

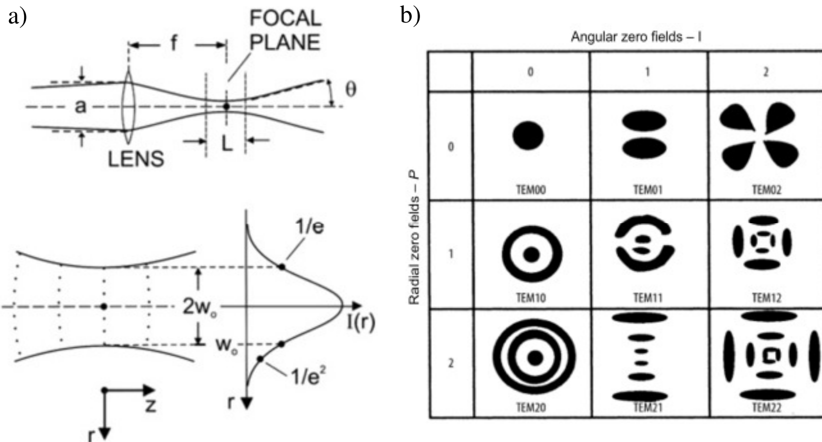

Source: [3, 5].

For a Gaussian beam profile (TEM00), the laser beam intensity within the focal plane has the form:

$$I(r) = I_0 e^{\left(-\frac{r^2}{w_0^2}\right)}, \qquad (2.1)$$

where r is the distance from the center of the beam and I_0 is the intensity for $r = 0$. w_0 is the radius of the laser focus, defined as the distance from the beam axis where the intensity has fallen to 1/e of the intensity on axis. Frequently, a similar parameter (w_e) is used. w_e is defined as the distance from the beam axis where the intensity has fallen to $1/e^2$ of the intensity on axis [1, 5].

2.1.4 Operating Mode

Lasers also have modes of operation. In the continuous wave mode (cw) the gain medium is pumped uninterruptedly and emits a temporally continuous laser beam. In the pulsed mode the beam is intermittently emitted in form of pulses [4, 6].

When operating in pulsed mode some parameters become important, such as the pulse repetition rate (f_{rep}), the duration of each pulse (τ_l), known as pulse width or pulse length and the peak power, that is the rate of energy flow in every pulse [7]. These parameters are related by equation:

$$P_{peak} = \frac{P}{\tau_l f_{rep}}, \qquad (2.2)$$

where P is the laser average output power.

Pulsed lasers are preferred in applications that require high heating rates and well-defined localization of the energy input within the workpiece. By using special pulse stretching and compression techniques, ultrashort pulses of picoseconds and femtoseconds can be achieved [5].

2.2 LASER ABLATION

In production technology, there are different strategies to achieve the final shape of a part. These strategies, known as manufacturing processes, can be classified in six main groups, according to the DIN standard (Figure 3): original forming, transforming, separating, joining, coating and finishing and change of material properties. The main group separating includes, among others, material removal operations, which can occur by different mechanisms and tools [8, 9].

Material removal comprehends the dissociation in non-mechanical means from particles of a solid body. It refers to the removal of layers of material as well as to the separation of workpiece parts.

Thermal removal using laser beam as tool, specifically, describes the separation of material by necessary heat provided by laser radiation to produce a required effect or shape. It comprises laser cutting and laser removal (also called laser ablation) procedures [8, 10, 11].

Figure 3 – Partial classification of manufacturing processes according to DIN 8580 and DIN 8590. Some subgroups are hidden to facilitate understanding.

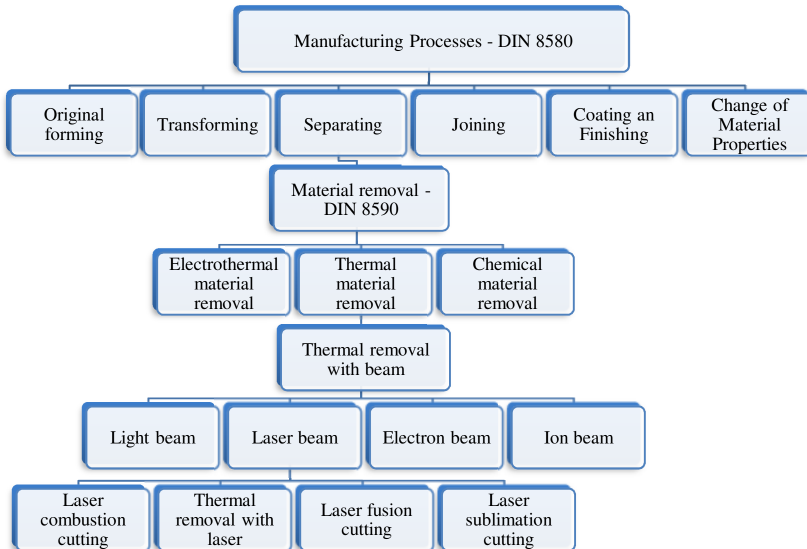

Source: Adapted from [8, 9, 11].

Laser ablation is a generic term that encompasses different applications like laser structuring, cleaning, drilling, machining, marking etc. Laser structuring means the production of complex structures in the surface to alter its properties (e.g. frictional coefficient or reflectivity). Laser cleaning stands for the removal of impurities, as well as of cover layers of the basis material. Laser drilling implies in the production of holes, predominantly with round geometry and high precision of removal. Laser marking means the manufacturing of visible marks on parts, e.g. bar codes, logos. Laser engraving expresses the generation of geometric forms (gravures, small cavities), with high volume of material removal and low precision [8, 4, 12].

Variations in laser parameters and material cause changes in the mechanisms of removal. Many models try to describe laser ablation by a

single dominant mechanism (thermal, mechanical, photophysical, photochemical and defect models). A more general description considers the simultaneous interaction of the different mechanisms and the coupling between them. Figure 4 shows the different interaction and feedback mechanisms of pulsed laser ablation. The process can be based on thermal activation only (left path), on direct bond breaking (photochemical ablation – right path), or on a combination of both (photophysical ablation – intermediate path) [5].

Figure 4 - Interaction between laser ablation mechanisms.

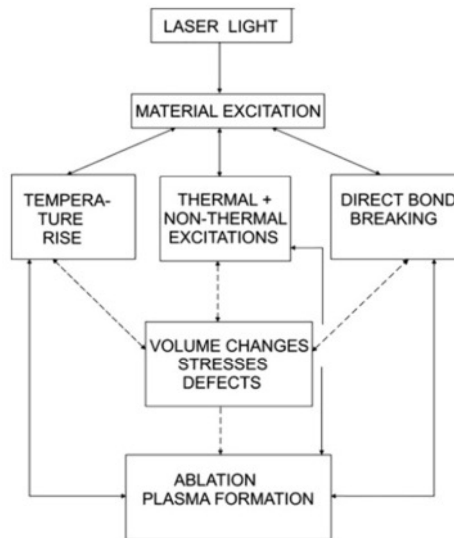

Source: [5].

2.2.1 Definition and Working Principle

Laser ablation is defined as the removal of material from a target of interest by direct absorption of laser energy [13]. The technology has gained space lately with the introduction of high powerful ultrashort pulse (USP) lasers. These lasers produce pulses of high power, with energy density so high, that the material can only absorb by evaporating or flying apart [3].

The laser beam is guided and focused on the workpiece surface by optical components. A thin superficial layer of the workpiece absorbs high power laser pulses. Due to the high energy density of the pulses, the material practically vaporizes, without passing through a liquid phase (it sublimates). Very little molten material and a very little heat-affected zone in the substrate result from the process [3, 14].

Figure 5 shows the laser-induced surface melting, vaporization and liquid-phase expulsion during laser ablation with ns pulses or longer. In the case of ablation with shorter laser pulses the liquid phase and the plasma plume are diminished or even avoided.

Figure 5 - Basic principle of laser ablation.

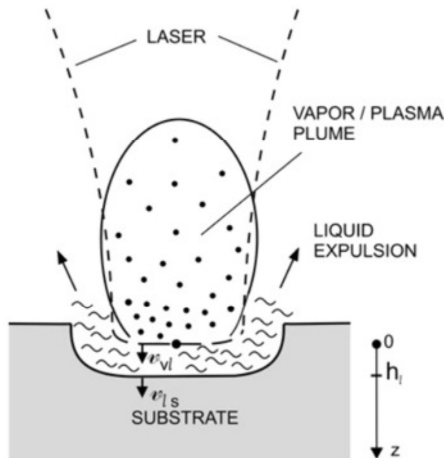

Source: [5].

Ablated shapes can be achieved using a mask or a scanner. In the mask technique the mask defines the exposure area at the workpiece (sample) and the desired shape is projected on the surface of the workpiece. The method is used, for example, in microelectronic industry using excimer lasers [12, 15]. In the scanner technique two moving mirrors, with perpendicular axes of rotation to each other, deflect the laser beam on the x and y-axis. An objective (flat field lens or f-theta lens) focuses the deflected beam, allowing the focus to be guided to any point within the working surface. In this method larger structures are

produced by overlapping individual laser pulses to form lines (tracks) and by combining tracks to create areas. The desired depth of the depression is achieved by processing successive layers [3, 4, 14]. Figure 6 displays the laser ablation process using mask and scanner.

Figure 6 - Laser ablation with mask (a) and scanner (b).

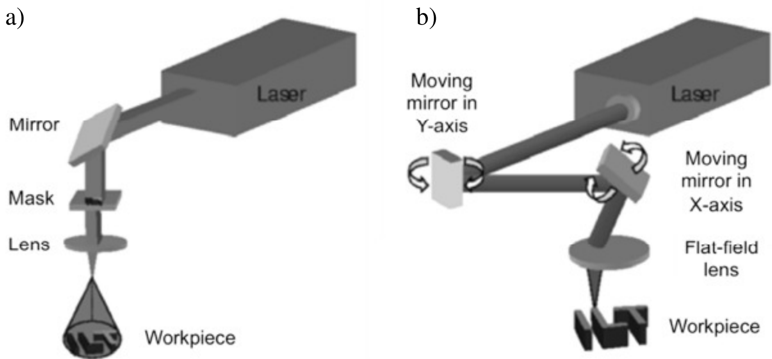

Source: Adapted from [12].

Figure 7 illustrates a scheme of the laser ablation process. V_s represents the scan speed, i.e. the speed in which the pulses advance to generate tracks.

Figure 7 – Laser ablation process scheme: a) single pulse; b) track; c) area.

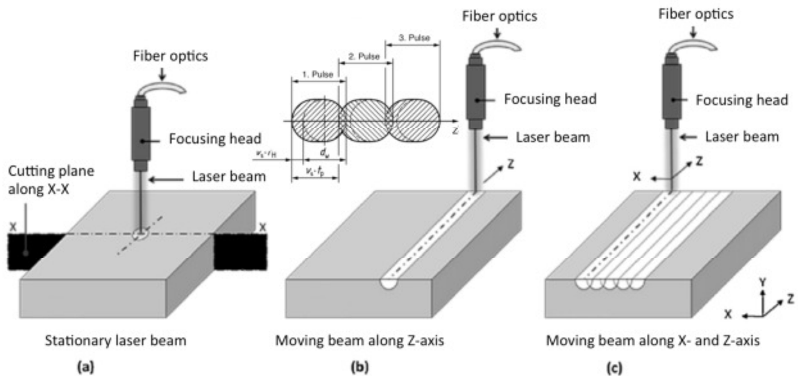

Source: Adapted from VORA et al. (2012) and DIN 32540 *apud* [16].

Laser ablation process characteristics allow operating on very fine structures causing very little chemical or mechanical damage, as well as working with cleanliness and precision [3].

2.2.2 Theoretical Background

Laser light is an electromagnetic radiation. When it strikes a surface different phenomena take place, such as reflection, absorption, scattering and transmission. Radiation and material properties will define the amount of energy in each phenomenon. Most of laser applications are based on the absorption of laser radiation by material and successive heat, melting, vaporizing or plasma formation. The absorption of radiation intensity by material follows, generally, the Beer-Lambert law:

$$I(z) = I_0 e^{-\propto z}, \quad (2.3)$$

where I_0 is the intensity that enters the workpiece, z is the distance that radiation travels inside the material and α is the absorption coefficient of the material, which depends on the medium, wavelength and intensity of the radiation [3, 16]. The distance after which the intensity is reduced by a factor of 1/e (~36%) is called absorption length or optical penetration depth l_α. It is defined as the inverse of the absorption coefficient [17]:

$$l_\alpha = {}^{1}/_{\alpha} \quad (2.4)$$

Electromagnetic radiation is associated to an electric and a magnetic field. When the radiation passes over a charged particle, the electric field induces a force that sets the particle in motion, initiating a forced vibration. This force is not high enough to move atomic nucleus, but it is capable of moving free or bound electrons. The phenomenon of photons being absorbed by electrons is known as the “inverse bremsstrahlung effect”. The vibrating electrons will either re-radiate in all directions (reflected, transmitted and scattered radiation) or be restrained by the lattice phonons (the bonding energy in a solid or liquid structure). In the case of the photons being restrained, the energy will be considered absorbed and the phonons will cause the vibration of the structure. As the molecules of the structure are linked, normal diffusion-type processes will conduct the vibration through it. This vibration is

identified as heat. If more energy is absorbed, more vibration will occur and the molecular bonding will be stretched, loosing mechanical strength and causing the melting of the material. On further heating the molecular vibration is so strong, that the material is said to have evaporated. If the vapor absorbs enough energy, it will become plasma [3].

Pulsed lasers are employed in practically all laser ablation applications. In these cases, the pulse width is a parameter that has a significant effect on the dynamics of the ablation process. In general, as the pulse width is shortened, energy is deposited faster into the material, leading to a rapid ejection, since it has less time to interact to the surrounding material. The low interaction to the surrounding material results in ablated features with more precision and less heat affected zone (HAS) [18].

Moreover, when working with ultrashort laser pulses, usually in the order of several picoseconds and femtoseconds, new phenomena take place. Plasma shielding is intensely diminished or even avoided, since material excitation occurs mainly prior to the expansion of the plasma plume. Thermally induced defect formation and decomposition inside the material volume occur in inorganic insulators and organic polymers. In higher laser intensity and/or shorter laser pulses, nonlinear optical processes and non-equilibrium effects become more important. Multiphoton processes increase the absorption coefficient and decrease the threshold fluence. Coulomb explosion is also noticed as an ablation mechanism. Femtosecond lasers when processing metals generate a hot electron gas in a cold lattice. The two-temperature model describes this transient non-equilibrium. Single-photon and/or multiphoton as well as impact (avalanche) ionization generate hot electron-hole pairs in semiconductors [5].

For ultrashort pulse laser ablation the duration of the pulse is shorter than the time required for relaxation (expansion) of the interaction volume. Thus, heat diffusion is “frozen” during the interaction of the laser beam with material and shock-like energy deposition leads to ablation [5, 13].

Figure 8 compares craters ablated by laser pulses with different pulse width. The craters formed by fs laser pulses are cleaner, with well-defined edges. The crater formed by ns pulses shows more irregularities due to the resolidification of splashed melt layers [13].

Figure 8 - Influence of the pulse width in laser ablation of steel foil. For laser pulses at 780 nm: a) τ_l = 200 fs, F = 0,5 J/cm^2; b) τ_l = 80 ps, F = 3,7 J/cm^2; c) τ_l = 3,3 ns, F = 4,2 J/cm^2.

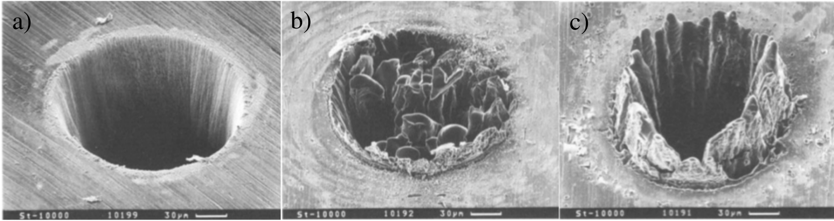

Source: [19].

In optics, fluence F represents the optical energy delivered per unit area (e.g. J/cm^2). In the same way, optical intensity I characterizes the optical power per unit area (e.g. W/cm^2). Both parameters can be related by $I = F/\tau_l$. For the laser radiation to ablate a workpiece, the fluence (or intensity) must be higher than the ablation threshold fluence (or ablation threshold intensity) of the material, that is the minimum energy density (or optical intensity) required to significantly remove material by ablation [20, 21]. Assuming a Gaussian distribution of the laser beam, rearranging equation 2.1, the ablated diameter can be expressed as [16, 22]:

$$D^2 = 2{w_0}^2 ln\left(\frac{I}{I_{th}}\right), \quad (2.5)$$

where w_0 is the laser spot size, I is the intensity and I_{th} is the threshold intensity. This way it is possible to ablate features smaller than the spot size, since only the areas subjected to energy densities higher than the threshold fluence will undergo ablation. This characteristic can be observed in Figure 9. For Gaussian spatial distributions with different intensities, only regions of the beam above the ratio I/I_{th}, (line on 1,0) are able to ablate material [12, 22].

Figure 9 - Relationship between beam intensity and ablated diameter.

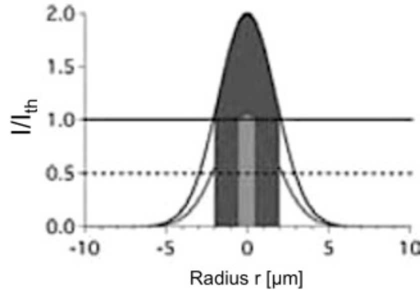

Source: Adapted from [12].

The ablation depth h is determined by material properties, like the absorption length and the heat of vaporization, as well as by laser beam properties, like energy density, laser pulse duration and laser wavelength [23]. For a single laser pulse with Gaussian distribution the ablation depth can be shown as [12]:

$$h = l_{\alpha} ln\left(\frac{I}{I_{th}}\right) \tag{2.6}$$

Operating close to the threshold intensity only small amounts of material will be removed. Increasing the intensity more material will be ablated, but heat propagation will arise [22].

2.2.3 Applications

Ultrashort pulse lasers, which can operate on very fine structures causing very little chemical or mechanical damage, have shown to be an important tool for material processing. Its characteristics, as well as the ability to work with cleanliness and precision has opened for laser ablation a growing niche market in surgical applications, lithography, micro-optical and electronic device manufacture, cleaning, among other applications [3].

Compared to other removal processes, like electrical discharge machining (EDM) and mechanical operations (e.g. drilling), laser ablation shows advantages and disadvantages. Table 1 compares different removal processes. The symbol “+” represents point of merit and “-” point of disadvantage. The inferiority in quality and accuracy

related to the other processes comes from the lack of a hard geometrically controlled edge that tools provide and the production of residual melt volume that clings to the machined edge [10].

Table 1 - Comparison of different removal processes.

Property	Laser	EDM	Mechanical
Rate	+	-	+
Quality	-	+	+
Scrap Management	+	-	+
Metal & non metal	+	-	+
Accuracy	-	+	+
Burrs	-	+	-
Equipment cost	-	-	+
Operating cost	-	-	+
High volume	+	-	+
Flexibility	+	-	-
Tool wear	+	-	-
Automation	+	+	+
HAZ	-	+	+
Clamping	+	-	-
Tool changes	+	-	-

Source: [10].

New developments in ultrashort pulse lasers and optics have improved the quality and accuracy of laser ablation procedures. The use of picosecond and femtosecond lasers allows very localized material removal due to low or practically no screening of the laser light along with low or practically no heat conduction within the material. This way it is possible to structure high thermal diffusivity materials (thermally high conductance) as well as wide-bandgap (crystalline) materials, glasses and polymers [5]. Examples of applications of ultrashort pulse laser ablation are:

- Thin film structuring: many innovative materials are based on thin films of conductive, semi-conductive or insulating materials deposited on glass or foils (Figure 10-a). The layers of the deposited material exhibit thickness in the micro and nanometer range. Examples of products made with multiple layers of such films are screens for smartphones, flat

lightning elements and flexible solar modules. The functionality of these components is determined by two-dimensional structures inside the film itself, which can be generated flexibly and economically by means of laser radiation [5, 24].

- Machining of Organic Light-Emitting Diodes (OLEDs): the patterning of one or more layers requires selective removal of material without depositing debris. This is difficult, but has been achieved with picosecond and femtosecond pulses. For example, aiming to avoid degradation when in contact with air, OLEDs are encapsulated by barrier layers that must be locally and selectively removed on the electrical contacts. The properties of the electrodes, however, may not be changed by the ablation [3, 24]. Figure 10-b shows flexible multicolor OLED on foil of stainless steel.
- Drilling: laser radiation is used to drill very small hole geometries (Figure 10-c), large aspect-ratio and ultra hard materials, where conventional process cannot be applied for. Applications are found in filter technology, photovoltaics, fuel-injector nozzles etc. [5, 25].
- Fabrication of medical implants: laser fine cutting of precise metal parts allows the manufacturing of medical components such as metallic stents (Figure 10-d) used as cardiovascular implants. Contactless processing and cutting kerfs of few micrometers make possible the manufacturing of very filigree parts [5, 25].
- Surface functionalization: structures can amplify intrinsic properties of selected materials or cause a specific effect by their structure size. With nanostructures optical functions (e.g. holographic gratings), biological functions (e.g. cell guiding structures) and analytical functions (e.g. specific molecule coupling areas; lab-on-a-chip engraving) can be achieved, for example. The technology is also used to alter reflectivity and to produce hydrophobic surfaces (e.g. lotus effect), shown in Figure 11-a; lubricant dimples in surface store lubricants (Figure 11-b), which can reduce friction; depressions with a lot of burring to increase friction; special characteristics in molds surfaces (Figure 11-c and Figure 11-d) etc. [4, 5, 25, 26].

Figure 10 - a) Free form ablation of thin films. b) Flexible multicolor OLED on foil of stainless steel. c) Shaped holes produced by 5-axis-trepanning. d) Laser cutted stent from stainless steel with details geometries < 100 µm.

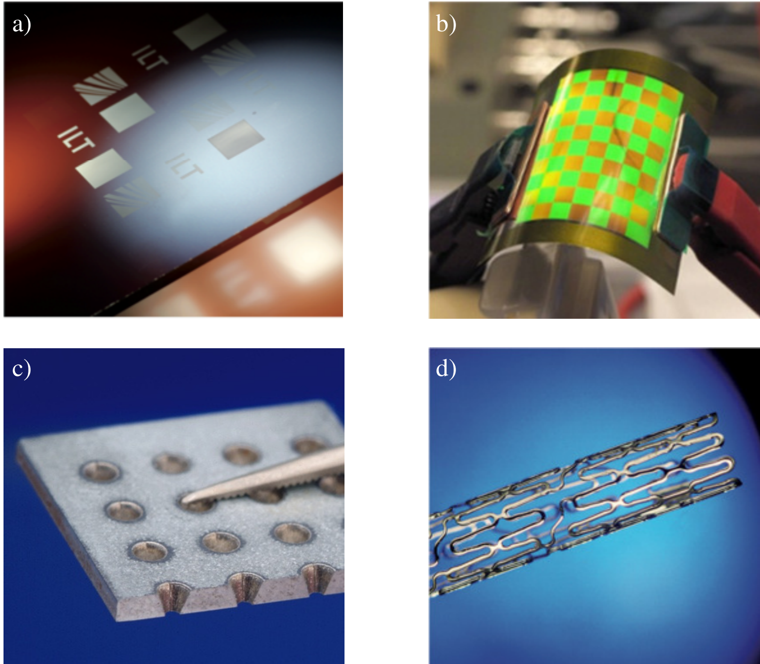

Source: Fraunhofer ILT; University of Stuttgart.

- Micromachining of materials for micro-optical and optoelectronic devices such as micromirrors, lens arrays (Figure 11-e), special lenses etc.
- Laser Induced Breakdown Spectroscopy (LIBS): LIBS is a rapid chemical analysis technology that uses a short pulse laser to create a microplasma on the sample surface. The radiation emitted from this plasma is analyzed to detect the presence and concentration levels of elements in the period table [27].
- Ablation of soft and hard biological tissues: ablation procedures using ultrashort pulse laser have been developed and used in many fields of medicine, including cardiology,

ophthalmology, dermatology, orthopedics, urology and dentistry, for example for caries removal [28, 29].

Figure 11 - a) Super hydrophobic surface microstructured with picosecond laser. b) Laser structuring of cylinder for improvement of tribological characteristics. c) Nanostructured hot-embossing roll made of heat-treated steel. d) Mold textured by laser ablation. e) Light guiding structure made of micro lenses for a uniform light distribution.

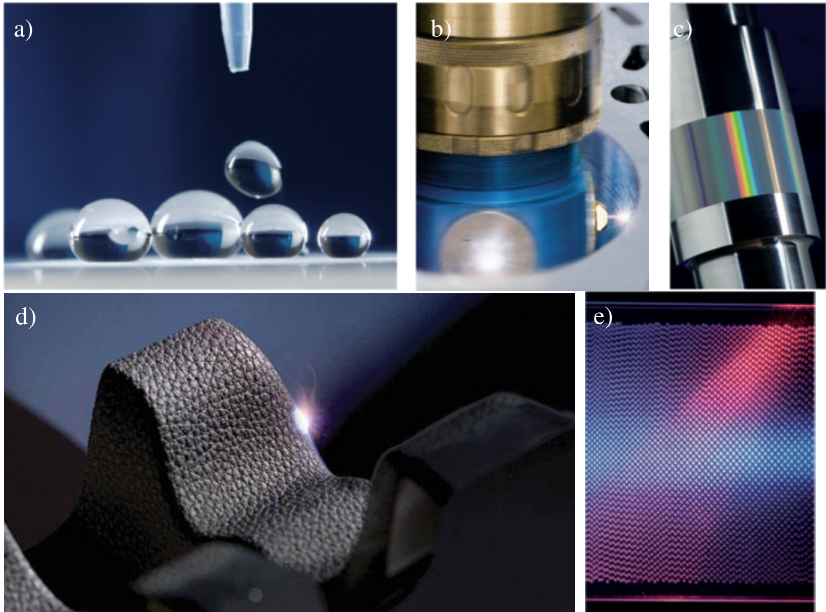

Source: Fraunhofer ILT; Gehring GmbH & Co. KG; Mold Making Technology.

Ultrashort pulse lasers have introduced new possibilities in the material processing as well as a new scale of working, that of nanotechnology. Picosecond and femtosecond lasers have shown to be important tools in the progress of technology [3].

2.3 LASER ABLATION IN PRINTED CIRCUIT BOARDS

With the advance of the electronics industry, devices moved from vacuum tubes and relays to silicon and integrated circuits. The increasing use of electronics in consumer goods brought the need for

size and manufacturing costs reduction. Printed circuit boards (PCBs) came as the solution for these issues [30].

Printed circuit board is a self-contained module of interconnected electronic components present in practically all electronic products, from common beepers to smartphones or computer systems. A PCB allows signal and power to be routed between physical devices through conductive paths called tracks. The circuits are formed by a thin layer of conducting material deposited on the surface of an insulating board, known as substrate. Solder connects electrically and physically the components to the surface of the PCB due to its conductivity and strong mechanical adhesive characteristic [30 – 32].

PCB construction can be classified as single-sided, double-sided or multi-layered. Single-sided boards have the components on one side of the substrate, while double-sided construction uses both sides. The latter one is employed when there are too much components for a single-sided board. Holes drilled through the substrate and plated with conductive material connect electrically each side of the board. These plated holes connecting different layers are called via (vertical interconnect access). Multi-layered boards are made of layers of conducting material separated by layers of insulation. Circuit patterns are simplified, since the components on the surface are connected through plated holes drilled down to the proper circuit layer [31, 32].

There are two methods to connect the components to a printed circuit board: the “through hole technology” and the “surface mount technology”. With the former one each component has thin wires, which are pushed through small holes in the substrate and soldered to connection pads in the circuit on the opposite side. This technology demands an extra step in the manufacturing process to drill the holes in the substrate, what leads to more time and production cost. With the latter one J-shaped or L-shaped legs on each component contact the printed circuits directly. The components are usually assembled by automated machines and consume less space than the connection pads from through hole technology [31, 33].

Regarding the materials, substrate can be made of paper reinforced phenolic resin, less expensive and often used in household electrical devices; polytetrafluoroethylene (PTFE), known by the brand name Teflon®; polyimid (PI), which has the advantage of being flexible; fiber reinforced glass (fiberglass) epoxy resin, ceramic etc. Fiberglass epoxy resin is the most frequently used substrate material. It combines good mechanical properties with near zero water absorption, but it is more expensive than paper reinforced phenolic resin. The designation

for fiber reinforced glass epoxy resin substrates is FR-4 (FR means flame retardant). The conducting material is generally copper, by reason of its excellent electrical conductivity and good mechanical characteristics. A thin copper foil is deposited on the substrate. The thickness is controlled in ounces per square foot (e.g. ½ ounce per square foot corresponds to 17,5 µm, 1 ounce per square foot corresponds to 35 µm). PCBs that handle high power may have thicker copper layers [30, 31, 33, 34].

According to Lewis and Ryan [35] there are three methods to produce circuit patterns in printed circuit boards: the subtractive method, the additive method and the semi-additive method. In the subtractive method copper layer is previously applied on the substrate, covering the entire board. Then, unwanted copper is selectively removed leaving only the desired circuit pattern. The typical subtractive procedure is to pattern circuits by photolithography using a photo mask and etch them away with a chemical solution, but there are others techniques like milling, laser ablation [36, 37]. The additive method uses electrolysis plating techniques to deposit the interconnecting pattern on the unclad starting board, while the semi-additive uses a combination of the two techniques, where the starting board has an initial thin deposition of copper on the surface of the board [38] *apud* [35]. After patterned and assembled, a solder resist mask is applied to the PCB to prevent subsequent oxidation and short-circuits [39].

The trend for further miniaturization in electronic devices foresees rigid and flexible circuits in dimensions that cannot be produced economically with the current technology. The demand for telecommunication and wireless-enabled devices, for example, has resulted in an overwhelming need for high density interconnect (HDI) circuits, with higher wiring concentration per unit area than conventional PCB. Applications like automotive displays, computer hard disk drives, flat panel displays, medical devices etc. also require HDI with vias and tracks in diameters and widths of few micrometers. The characteristics of laser beam meet these needs and for this reason laser technology has proven to be suitable in printed circuit boards manufacturing, especially for producing HDI structures. With the development of new laser equipment with small spot size and accurate energy control it is possible to use laser light to drill, to structure and to cut PCBs [40 – 42].

Laser is capable of drilling a variety of materials, therefore it is used to created microvias by opening the copper layer and removing the substrate (Figure 12-a). Hole diameters of less than 50 µm can be

produced with high precision, ideal geometry and positional accuracy. The ability of processing practically all PCB materials also enables clean cutting of fine contours in different material thickness with no burring and minimal thermal influence (Figure 12-b). The contact-free processing avoids distortion. Flexible, flex-rigid and thin multilayers can be cutted [39, 40, 43, 44].

Laser radiation is also used to image a pattern directly onto a panel coated with photosensitive resist. The laser beam is scanned across the photoresist surface and switched on and off according to the electrical circuit pattern. It eliminates the production and use of traditional photo tools (masks), what saves time and costs in the manufacturing process. This technology is known as Laser Direct Imaging (LDI) and makes possible the fabrication of very fine structures (e.g. microfluidic applications), correcting distortion, shrinkage or positional errors caused by conventional photolithography method [45 – 47]. Figure 12-c shows an example of tracks pattern made by LDI.

Another alternative in the use of laser in PCBs is the structuring of standard resists, used in conventional photolithographic imaging processes of panel plating and pattern plating by removing, respectively, the etch resist and the plating resist. Laser can also ablate solder resist masks and foils as well as chemical tin resists for the production of ultra-fine lines. In the latter case (Figure 12-d), after removing the tin-resist coating and part of the copper layer, the remaining copper is etched. This technique does not require the photolithography step and allows the production of lines with resolution of < 50 µm. Laser structuring of resists is recommended for the production of high density areas with fine resolution on HDI printed circuit boards. The majority of the board is still manufactured conventionally by photolithography [48, 49].

Figure 12 - a) Microvia in resin coated copper D = 75 µm. b) Laser cut flexible printed board. c) Magnified HDI circuit area patterned by LDI. d) 50 µm tracks/gaps on Cu base material.

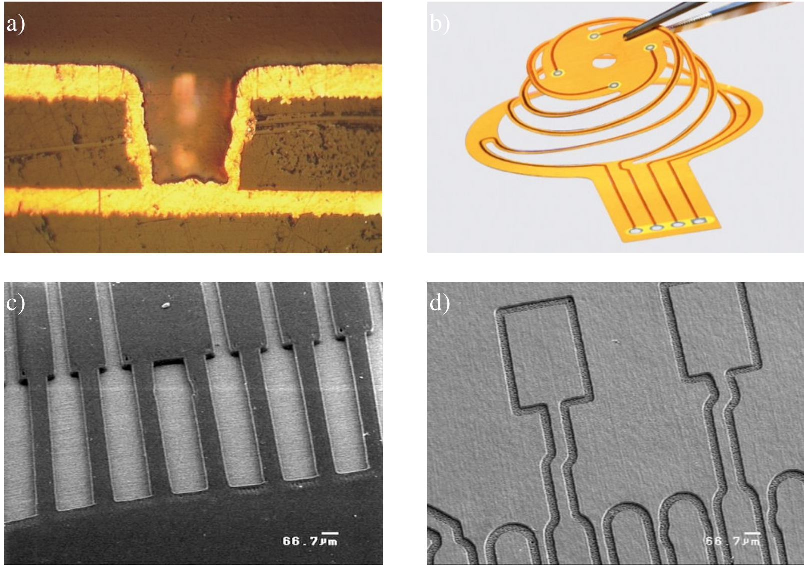

Source: LPFK Laser & Electronics AG.

Direct structuring circuit layouts by laser ablation of conductive layers is an important application of laser in PCBs. In a subtractive process, a high energy density laser beam removes the conductive layer precisely creating insulation channels, tracks and pads. Advantages include high flexibility, high repetition accuracy, precise geometry, fast processing and the ability to process various materials. During processing no photo masks or chemicals are required. Laser structuring of conductive layers has been applied in complex digital and analogue circuits as well as in radio frequency and microwave circuits, for the production of antennas, filters among others. The process is suitable for the manufacturing of individual components with high variance and for small series production [39, 50 – 52]. Figure 13 exemplifies a sample of laser structured PCB as well as the laser processing unit.

Figure 13 - a) Laser structured PCB sample. b) ProtoLaser U3 processing unit.

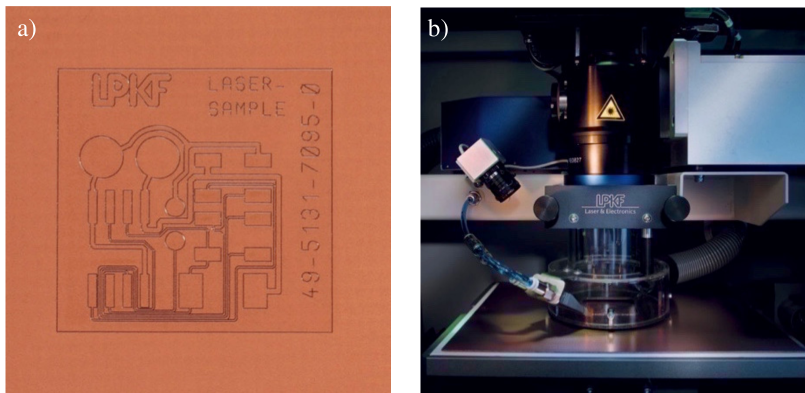

Source: LPKF Laser & Electronics AG.

In 3D molded parts circuit tracks can be produced on the part surface, combining electrical and mechanical functions in a single construction unit. These components are called molded interconnect devices (MIDs). To process MIDs LPKF created the Laser Direct Structuring (LDS) method, in which the laser structures the tracks on a 3D injection-molded part made of polymer material. The structures are then metallized in a subsequent step. The technology is used in automotive, consumer and medical applications [53, 54].

2.4 PROCESS MONITORING

Manufacturing today requires a high level of quality and productivity to be competitive. Ideally, laser material processes are designed such that they achieve a constant level of quality for all kinds of products that they produce. However, the number of parameters for the laser material process is large when properties of the laser beam and the product's geometry, for example, have to be taken into account. Under these boundary conditions, when stable process parameters cannot be defined, process monitoring is a promising approach to track the current state of the process during processing.

Process monitoring is a method to achieve quality assurance for a product and/or process. It is also used in scientific environment to gain a better understanding of the interaction process of the laser radiation and

the material. This is made by observing the behavior of a process by means of interim and trend information [55, 56].

Different strategies can be applied in process monitoring: off-line monitoring, on-line monitoring and closed-loop control. Off-line monitoring processes the data off-line, allowing the creation of a quality report or certificate for the respective product. On-line monitoring systems will immediately create failure messages in case of detected not allowed process irregularities. Closed-loop control systems are designed to continue the process by applying appropriate feedback to allow taking actions for compensating a beginning decrease in product quality [56].

In laser process monitoring, there are different ways to make tests and measurements of process variables and defects. These measurement methods can be separated in three categories, depending on "when" they are applied: pre-process, for activities executed before the process takes place, like measuring thickness of a metal sheet, examining the components of an alloy etc.; in-process, for everything that is done during processing, like on-line monitoring and process control and post-process, for what is done after the process takes place, like analyzing process data or reviewing process imaging through video files.

The quality of a laser process is judged by directly or non-directly assessable criteria, e.g. occurrence of pores and seam geometry in laser welding or roughness of the cut face in laser cutting. The quality criteria are evaluated by output phenomena (e.g. electromagnetic radiation emission from the interaction zone), detected by sensors and characterized quantitatively by output parameters (e.g. spectral frequency pattern) [56]. The design of a process monitoring system can be grouped in the following decisions:

1. How is the quality of the process / product defined?
2. Which process variables determine process/product quality?
3. Which measurands can be captured?
4. How can process variables be correlated to process measurands?

Lateral or coaxial sensors can make the surveillance of processes. The sensor can be a photodiode, electronic camera, microphone etc. Through optical components, events from the interaction zone are captured and sent to an integrated computer for analysis. It is also possible to combine different sensors, such as camera and photodiode, and correlate the signals for evaluation.

Figure 14 - Lateral (left) and coaxial (right) arrangement for laser process monitoring.

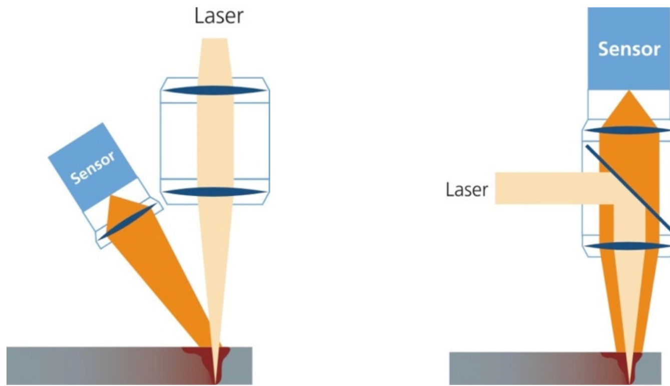

Source: Fraunhofer ILT.

In lateral systems, the sensor and the working laser beam are not on the same optical axis. It is usually a faster and simpler way to mount a system. Lateral implementations also allow the observation of regions of the interaction zone without interference of vapors and/or plasma emitted by the interaction between laser and workpiece.

In coaxial systems, the sensor and the working laser are on the same optical axis. This arrangement needs special optical components, such as dichroic mirrors. The technique of coaxial process monitoring and control systems for laser applications was pioneered by Fraunhofer ILT and is closely linked to their CPC brand (coaxial process control).

Coaxial sensors obtain information independent from feed-direction, since the sensor always captures data from the interaction zone of laser and workpiece. It acquires either a spatial or integral signal from the processing zone. CPC systems can be used in all laser applications, like cutting, welding, surface treatment, additive manufacturing, laser ablation etc.

Applications of process monitoring for quality assurance have grown in laser industry, in processes like welding, cutting, drilling etc. and in scientific research, with the introduction of online monitoring to new processes, like laser metal deposition, selective laser melting and laser ablation to name only some.

2.4.1 Process Monitoring in Laser Ablation

In general, laser ablation technologies require high control of the parameters that can affect the process stability and the product quality. For manufacturing precision parts, extremely small tolerable parameters deviations are allowed. For this reason, the employment of process monitoring systems is crucial [57].

Different methods of process monitoring and control are available to ensure a stipulated quality during laser ablation process. For the depth measurement, optical coherence tomography (OCT) techniques may be highlighted. For materials diagnosis, several measurements procedures may be applied, such as reflection measurement and spectroscopic analysis [14].

2.4.1.1 Optical Coherence Tomography

Optical coherence tomography is a noninvasive optical imaging technique that provides 1D depth, 2D cross-sectional and 3D volumetric images of objects with depth resolution in micrometer-level. Light backscattered from different layers of material within a sample provide structural information of the sample to generate OCT images. The method is capable of creating real-time imaging. Its characteristics, like high resolution, great imaging depth and non-contact sensing make OCT suitable for imaging biological tissue, small animals and materials. Current developments in OCT have led to new methods based on low-coherence interferometry. These methods are known as Fourier domain optical coherence tomography (FD-OCT). There are two types of FD-OCT according to the light source and detection scheme used: Spectral Domain OCT (SD-OCT) and Swept Source OCT (SS-OCT) [58].

FD-OCT uses coherent properties of a light source to measure optical path lengths delays in a sample. A low-coherent light source directs light beam at a sample surface and at a reference arm with fixed optical path. Reflected light signals from both arms (sample and reference) are combined resulting in an interference pattern. The frequency of the pattern is measured by the sensor. Taking a Fourier transform of the detected interference pattern it is possible to obtain a depth profile (A-scan). Scanning across the sample enables collecting 2D cross-sectional image (B-scan). And scanning in the perpendicular direction 3D information of the sample can be obtained by combining multiple cross-sections [58 – 60].

Figure 15 - Scheme of Spectral Domain OCT (SD-OCT). FC means fiber coupler and CCD means charged-coupled device.

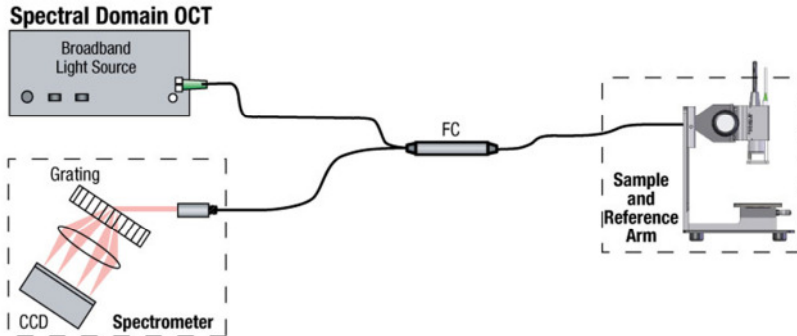

Source: Thorlabs.

FD-OCT has been employed in laser ablation to measure the macro-geometry of the surface before ablation as well as to measure the ablation depth in order to provide feedback to the controlling system of the machine that can readjust the process parameters for reaching best results [57]. It has also been applied for space resolved determination of ablation rates, contributing to a better understanding of the process and fine-tuning of the laser [60].

2.4.1.2 Spectroscopic Analysis

The use of spectroscopic analysis for process monitoring makes possible the acquisition of important information from the interaction zone between laser and workpiece during ablation. Since all elements emit radiation of characteristic frequencies when excited to high temperatures, measurements of elemental concentration in materials are possible by spectral analysis of the microplasma produced during laser ablation (Figure 16). This procedure is known by different names, like laser-induced breakdown spectrometry (LIBS), laser-induced emission spectral analysis (LIESA), laser-induced plasma spectrometry (LIPS) [61 – 64]. Among the advantages of laser-based analytical methods are noncontact measurement, high measurement speed, good lateral resolution (down to several µm) and no or practically no sample preparation [61, 62, 65].

Figure 16 - Basic set-up for laser-induced breakdown spectrometry.

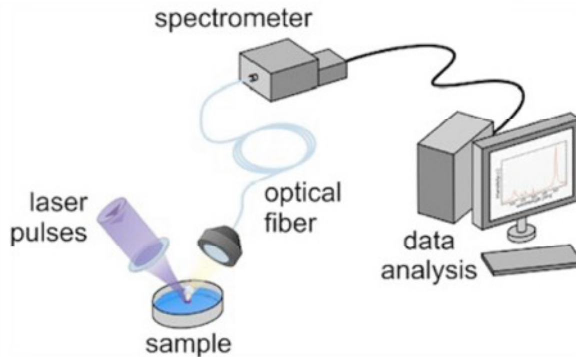

Source: Adapted from Tampere University of Technology.

Analysis of elemental concentration of materials have shown to be an important method of process monitoring in the production of steel, by the direct examination of the molten metal; in the verification of the elements distribution in polymers, by homogeneity measurements of tire rubber in the mixing shop; in the online control of geological raw materials on conveyor belts; as well as in the process of deposition of superconductors thin-films [63, 66].

With the examination of the emitted spectrum it is also possible to characterize the depth profile of multi-layers samples by the change in the detected spectral pattern [63 – 65]. Furthermore, spectroscopic analysis can provide, along with information about materials, knowledge about the ablation process, such as the ablation rate [65].

2.5 OPTICAL SPECTRUM ANALYSIS

The previously mentioned process monitoring techniques applied in laser ablation (OCT and spectroscopy) investigate the spectrum of the radiation emitted from the interaction zone between laser and workpiece to extract information about the process conditions. By means of optical components the light spectrum is separated as a function of wavelengths or optical frequencies and the power spectral density of the separated wavelengths is measured. The measurement of optical power as a function of wavelength is known as optical spectrum analysis [67, 68].

Optical spectrum analyzers are instruments designed to measure the power distribution of an optical source over a specified wavelength span. They can be categorized according to their architectures in interferometer-based and diffraction grating-based (or prism-based) [67, 69].

2.5.1 Interferometer-based Optical Spectrum Analyzers

Interferometer-based optical spectrum analyzers utilize the effect of interference of the light to carry out measurements of the power or spatial shape of the resulting beam. They provide high spectral resolution, but in a very limited spectral range [70, 71]. According to [67] the interferometer-based optical spectrum analyzers are classified in the Fabry-Pérot type and in the Michelson type.

2.5.1.1 Fabry-Pérot Interferometer

A Fabry-Pérot interferometer is a linear optical resonator, which consists of two high reflecting mirrors (with some transitivity) in parallel mounting. The light reflects multiple times between the two mirror surfaces and part of the radiation is transmitted every time the light reaches the second surface, resulting in multiple offset beams that can interfere with each other. The resonance frequencies can be tuned by changing the cavity length (mirror distance) [67, 72 – 74].

Figure 17 - Fabry-Pérot interferometer-based optical spectrum analyzer.

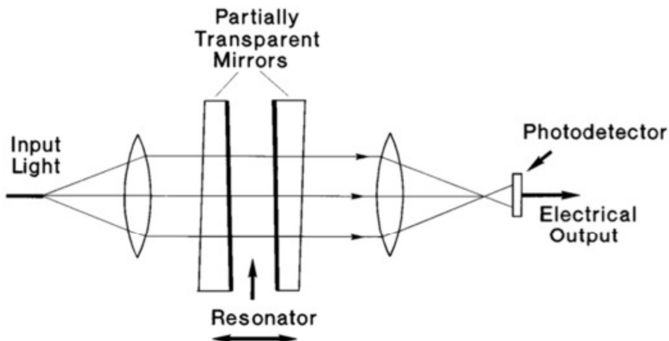

Source: Agilent Technologies.

The advantage of Fabry-Pérot interferometer is its very narrow spectral resolution. The disadvantages are a small wavelength range and at any position multiple wavelengths will be passed by the filter [67, 75].

2.5.1.2 Michelson Interferometer

In the Michelson interferometer the input signal is split into two paths by a beam splitter (partially reflecting mirror). The beams are then reflected by two mirrors, one fixed and the other one movable. When the reflected beams are brought back together the path length difference between them results in an interference pattern. The power of the interference pattern is measured. Performing a Fourier transform, the input signal is revealed in a wavelength range. Michelson interferometer is able to make direct measurements of coherence length, as well as very accurate wavelength measurements, being commonly used for wavelength meters. [67, 71, 75, 76].

Figure 18 - Michelson interferometer-based optical spectrum analyzer.

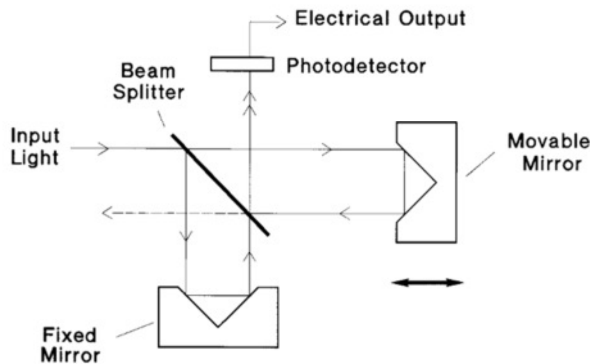

Source: Agilent Technologies.

Although scanning the entire wavelength range and having good wavelength accuracy, Michelson interferometers are weak in its ability to provide a large dynamic range [67, 75].

2.5.2 Diffraction Grating-based Optical Spectrum Analyzers

Diffraction grating optical spectrum analyzers use the wavelength-dependent diffraction on diffraction gratings to separate the optical spectrum. The effect is similar to the achieved with a prism, but diffraction gratings provide grater separation, with less attenuation, what leads to a better wavelength resolution. After meeting the diffraction grating the different components of the spectrum propagate in slightly different directions. The radiation may travel through additional optics until it reaches the detector [67, 70, 75].

Some grating spectrometers are very compact, however the highest performance, especially in terms of resolution and sensitivity, are achieved with larger instruments [70]. The high wavelength separation resolution of diffraction grating-based optical spectrum analyzers leads to applications for measuring atomic spectra in both laboratory instruments and telescopes [77].

Figure 19 illustrates a simplified scheme of a diffraction grating-based optical spectrum analyzer. The different wavelengths of the input beam are separated by the diffraction grating. Only part of the spectrum (selected wavelengths) passes through the aperture and reaches the detector. Tuning is possible by changing the diffraction grating angle. It allows different wavelengths to enter the aperture.

Figure 19 – Simplified scheme of a diffraction grating-based optical spectrum analyzer.

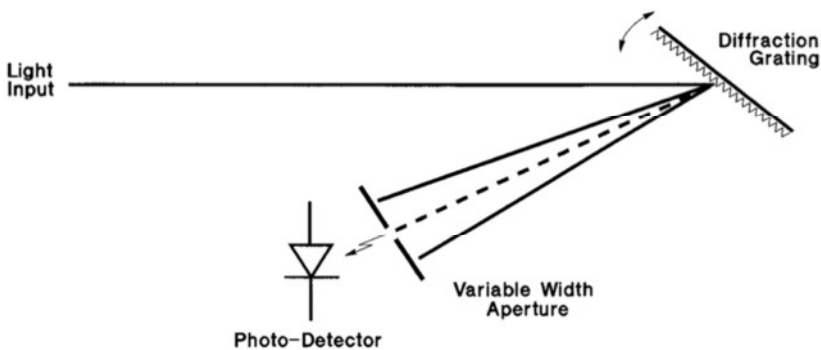

Source: Agilent Technologies.

Optical setups that select only one narrow range of wavelengths to get the detector at one time are known as monochromators [70]. Monochromators are generally compound by diffraction grating, apertures (slits) as well as additional optics, like curved mirrors. These optical setups will be detailed in the next sections.

2.5.2.1 Diffraction Grating

Diffraction grating is an optical device that plays an important role in spectroscopy due to its ability to separate polychromatic light into its constituent monochromatic components. It contains periodic structures (grooves) that cause varying optical amplitude and/or phase changes. Diffraction gratings can be classified in reflection and transmission gratings. The reflection grating consists of a grating superimposed on a reflective surface, whereas the transmission grating comprises a grating superimposed on a transparent surface [78, 79].

Gratings can also be categorized according to the manufacturing process. Ruled gratings are produced by physically forming grooves on a surface with a diamond tool mounted on a ruling engine. Holographic gratings are fabricated by creating constructive interference in a photolithographic process. Commercial gratings are usually made by a replication process, where a single master is produced, either ruled or holographic; and the three-dimensional topography of the master is transferred to another substrate, enabling reproduction with very close tolerances. Ruled gratings can be robust and present high diffraction efficiency, but they can cause substantial amount of stray light due to surface irregularities, what is a disadvantage when using in grating spectrometers [79, 80].

To improve efficiency of a grating the grooves - the individual reflective elements - can be inclined by an angle called blaze angle (γ). Changing the blaze angle concentrates diffracted radiation to a specific region of the spectrum, increasing the efficiency of the grating in that region. The wavelength at which the highest efficiency appears is called blaze wavelength. The angles of incidence (α) and diffraction (β) - the latter as a function of the distance (d) between successive grooves - will determine the angular dispersion of a grating [80, 81]. Figure 20 shows some parameters and angles of a diffraction grating. L is perpendicular to the grating surface. L' is perpendicular to the active flank.

Figure 20 - Diffraction of light at a diffraction grating.

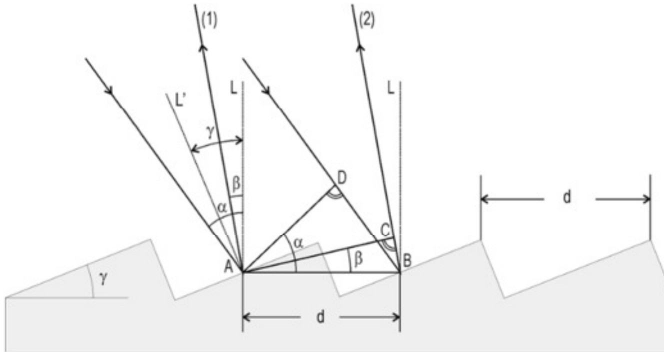

Source: [82].

The relationship between angles and grooving distance is expressed by the equation 2.5, where m is the diffraction order, which is an integer and λ the wavelength. For a specific wavelength λ, values of m for which $|m\lambda/d| < 2$ correspond to physically realizable diffraction orders [78].

$$m\lambda = d(\sin\alpha + \sin\beta) \quad (2.7)$$

For a particular set of values of d, α and β, the equation 2.5 is satisfied by more than one wavelength, generating various "orders" of diffracted radiation. Physically it means that the light reflected or transmitted off adjacent grooves undergoes constructive interferences, forming different diffracted order beams. For the constructive interference to occur, the path length difference between reflections or transmissions from adjacent grooves must correspond to one wavelength or some integral multiple thereof. In the case of a polychromatic incident beam, the angle of reflection or transmission must be different for each wavelength, in order to satisfy the requirement that the path length difference off adjacent grooves is equal to one wavelength. The order m=0 is a pure reflection and there is no wavelength separation. The first order m=1 corresponds to a path length difference between rays diffracted from adjacent grooves equals one wavelength. For the second order m=2 the path length difference is equal to two wavelengths. The

third order beam has a difference of three wavelengths and so on. There may be also negative orders [67, 78 – 80].

Figure 21 – Output beams of diffraction orders.

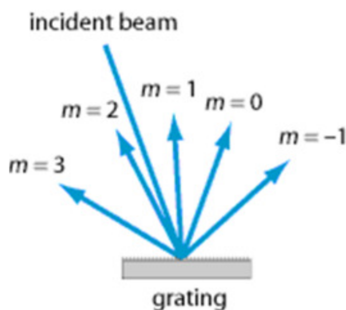

Source: [79].

At higher orders efficiency and free spectra range - maximum bandwidth in an order without spectra interference of adjacent orders - decreases whereas angular dispersion increases [80].

2.5.2.2 Monochromator

Diffraction gratings are widely used as dispersive element in monochromators. A monochromator is a device used to isolate a narrow wavelength region of the spectrum. In other words, a monochromator is a tunable bandpass filter for light in optical spectrum analyzers. It is employed to examine wavelengths and intensities of spectral lines emitted by a source [83, 84]. The quality of an optical spectrum analyzer basically depends on the ability to separate two closely spaced spectral lines, which is mainly determined by the internal monochromator [85].

The typical optical design of a monochromator essentially consists of an entrace slit, collimating and reflecting mirror, diffraction grating and exit slit. Light enters the monochromator through the entrance slit. A spherical mirror collimates the light and directs it to the grating. The diffraction grating disperses different wavelengths at different angles. These distinct wavelengths are focused by a curved mirror and one of them (or a small wavelength band) emerges from the exit slit. A detector can be placed after the exit slit for spectral analysis. By turning the grating, each individual wavelength can be imaged onto

the exit slit, enabling the detector to receive a spectrum [83, 86]. This design - shown in Figure 22 - is known as the Czerny-Turner configuration.

Figure 22 - Czerny-Turner configuration.

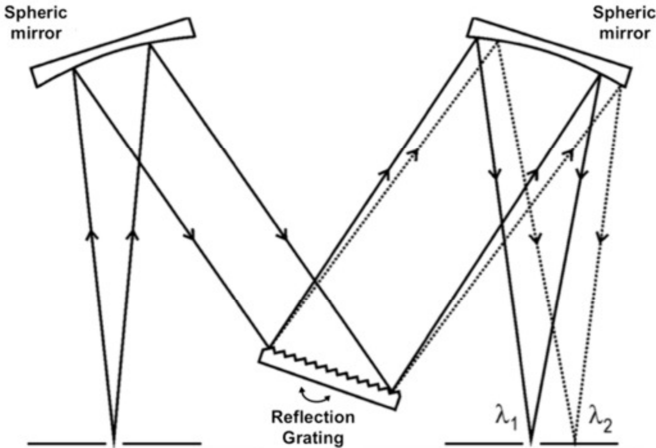

Source: Adapted from [82].

The resolution is influenced by the focal length of the monochromator, the dispersion of the grating and the width of the entrance and exit slits. Resolution is inversely proportional to the slit width. Narrow slit widths lead to higher resolution. On the other hand, large slit widths give rise to higher intensity signals, among with loss of resolution. Additionally, large entrance slit widths are more tolerant to misalignment [85 – 87].

Besides Czerny-Turner configuration (Figure 22), there are other designs, such as the Ebert-Fastie, the Rowland Circle and the Offner configuration. Ebert-Fastie configuration is a variation of the Czerny-Turner arrangement, for which two concave mirrors are combined into one large mirror. Figure 23 displays the optical arrangement of an Ebert-Fastie monochromator. Rowland Circle configuration (Figure 24) includes the entrance slit, a concave grating and one or more exit slits or point detectors. It enables different wavelengths to be measured through the simultaneous measurement of intensity at several points on the Rowland Circle. Using curved gratings it is also possible to design imaging spectrographs, where every point of the entrance slit can be

spectrally resolved on a flat detector. Offner spectrograph configuration – displayed in Figure 25 is basically a Czerny-Turner configuration with a convex grating instead a plane one. It allows high spectral and spatial resolution [88].

Figure 23 - Ebert-Fastie configuration.

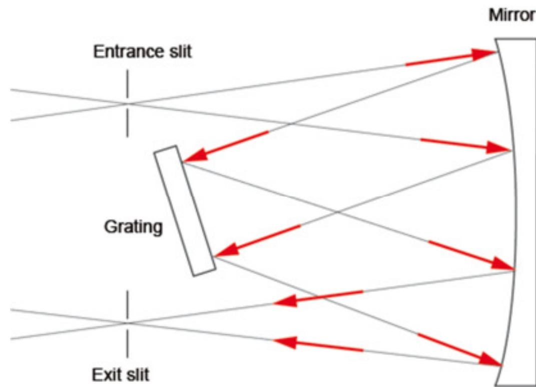

Source: [88].

Figure 24 - Rowland Circle configuration.

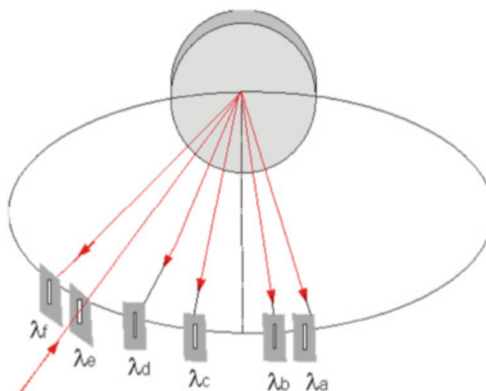

Source: [88].

Figure 25 - Offner configuration.

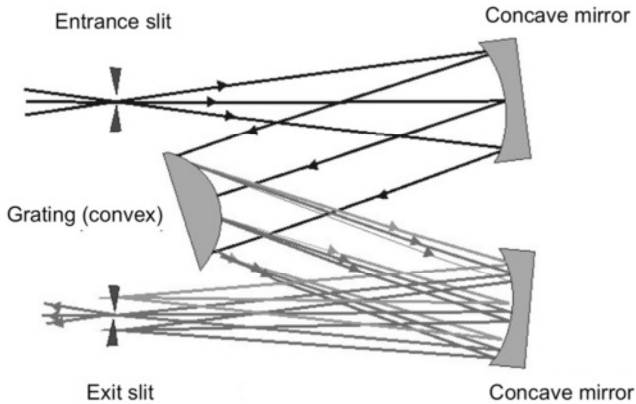

Source: Adapted from Carl Zeiss.

Configurations involving two monochromators connected in series are sometimes used to improve the dynamic range of single monochromators. However, these arrangements - called double monochromators – usually have reduced span widths due to the tuning match between both devices and degraded sensitivity due to losses in the equipment [67].

A scanning spectrometer can be assembled by placing a detector after the exit slit of the monochromator. In this case, only a small range of wavelengths will reach the detector at one time. For scanning a larger wavelength range, the slit position or the angular orientation of the grating may be moved. A wide spectral range acquisition with high resolution can take a long time. An alternative for a faster acquisition of spectrum is to place a spatially resolved detector (e.g. a CCD camera chip) on the exit plane instead of the exit slit. Thus, a wide range of the spectrum is simultaneously recorded by the detector [70, 86].

2.5.3 Photodetectors

Photodetectors are optical receivers that convert light into electric signal by means of the principle of the photoelectric effect. Photodetectors have an illuminating window covered with an anti-reflect coating to absorb light photons. The result of the absorption of photons is the creation of electron-hole pairs in the depletion region. The

transport of free electrons and holes upon an electric field results in a current [89, 90].

Photodiodes are commonly used photodetectors. These semiconductors devices contain a p-n junction, where light is absorbed in a depletion region and produces a photocurrent. Photodiodes can be operated in two different modes: photovoltaic and photoconductive. In the photovoltaic mode the illuminated photodiode generates a voltage that can be measured, whereas in the photoconductive mode a reverse voltage is applied to the diode and the resulting current is measured [91].

Some photodiodes, called p-i-n or PIN photodiodes, include an intrinsic (i.e. undoped) layer between the p and n doped regions. Compared to an ordinary p-n photodiode, a p-i-n photodiode has a thicker depletion region, what leads to larger quantum efficiency (percentage of incident photons that contribute to the external photocurrent) and higher detection bandwidth [89, 92]. Another variation is the avalanche photodiode (APD), designed to provide an internal current gain by impact ionization [93]. These devices operate with a relatively high reverse voltage. The strong internal electric field intensely accelerates the carriers (electrons and holes) excited by absorbed photons, generating secondary carriers and amplifying the photocurrent, in a phenomenon called avalanche process. The avalanche process increases responsivity (ratio of the photocurrent output to the incident optical power), but subjects the APD to quantum noise and introduces multiplication noise. Generally, when high detection bandwidth is required, the noise performance of APDs is better than that of regular p-i-n photodiodes. For lower detection bandwidth a p-i-n photodiode combined with a low-noise narrow-band amplifier can be more suitable [94]. Photodiodes can also be connected in a linear array on an integrated circuit chip. This assembly is known as photodiode array (PDA) and it is very useful to record a range of wavelengths simultaneously in a spectrometer [93].

Photomultiplier tubes (PMTs) are a particular type of photodetectors based on vacuum tubes. They can combine extremely high sensitivity with ultrafast response. A photocathode emits photoelectrons into vacuum when light is absorbed. The photoelectrons are directed by a focusing electrode voltage towards an electron multiplier where the electrons are multiplied by the process of secondary emission. The electrons are collected by an anode as an output signal. Due to the secondary emission PMTs provide extremely high sensitivity with very low noise. They also present ultrafast response among with

high bandwidth. These characteristics enable the use of PMTs in very low intensity applications, even for photon counting [95, 96].

Charged coupled device (CCD) is an integrated-circuit chip that contains an array of capacitors (cells) that stores charge when light creates e-hole pairs. The packets of charge are moved from cell to cell by the coupling and decoupling of potential wells within the semiconductor until the end of the line, where the charges from all cells are converted to electric signal. CCDs are used in similar applications to the photodiode arrays, but they are more sensitive at low light levels [93, 97].

Silicon photomultipliers (SPM) are detectors that address the challenge of detecting, timing and quantifying low-light signal down to the single-photon level. When a photon travels through silicon it creates an electron-hole pair. Under application of a reverse bias, an absorbed photon will result in a net current electrons through the n-type and holes though the p-type sides of the device. SPM combine high gain and low noise, among with ruggedness [98].

Single photodetectors may be employed at the monochromator output (e.g. photodiodes, p-i-n photodiodes, APDs, photomultipliers), according to the wavelength range and sensitivity required. To acquire simultaneously a wide spectral range, multichannel detectors, like photodiode arrays or CCDs, may be applied [86]

Other types of photodetectors are currently available, such as phototransistors, metal-semiconductor-metal (MSM) photodetectors and photoresistors to name only some.

3 METHODOLOGY

3.1 EQUIPMENT AND MATERIALS

The activities of this work were carried out at the Fraunhofer Institute for Laser Technology, in Aachen, Germany, as part of the joint project MaLDeAN. The CPC laboratory of the Process Control Group was used for the development of the conception, assembly and calibration of the prototype. At one of the laboratories of the Micro and Nano Structuring Group the system was integrated with the laser ablation machine and tested.

The ablation machine, the laser source and the optical spectrum analyzers used to characterize the optical elements are detailed in the next sections. Other equipment used in the construction of the system, such as optical components and detector will be described along the prototype development.

3.1.1 Laser Ablation Machine

The monitoring system was integrated with the machine SAUER LASERTEC 50 (Figure 26). It is a 5-axis highly dynamic precision machine suitable for laser ablation applications. The machine is combined with a picosecond laser source [99]. The beam is delivered to the workpiece surface by a set of mirrors, passing through a varioSCAN focusing unit, which can focus the beam onto a flat image field, a scan head (2D-scanner) that allows beam movements on the X and Y-axes and a flat field lens that also focuses the laser beam. The combination of the varioSCAN unit and the f-theta objective allows the achievement of large working volumes. The scan head, the flat field lens and some mirrors will be further detailed in section 5.1. A CCD camera and a 3D measuring probe system contribute to a fast setup.

Figure 26 - LASERTEC 50 (LT 50) machine platform.

Source: DMG MORI.

3.1.2 Laser Source

A TRUMPF TruMicro 5050 laser source was used for the ablation process. This laser source is able to produce high energy pulses below 10 ps. Table 2 shows some of the TruMicro 5050 characteristics.

Table 2 - Laser source characteristics.

Wavelength	1030 nm
Average laser power	50 W
Max. pulse energy	250 μJ
Pulse duration	< 10 ps
Repetition rate	200 – 800 kHz

Source: [100].

3.1.3 Optical Spectrum Analyzers

Spectral analyses of optical components were conducted with two instruments: an Ocean Optics HR2000+CG-UV-NIR spectrometer and a Perkin Elmer Lambda 1050 spectrophotometer.

HR2000 is a modular spectrometer with a 300 lines/mm grating and order-sorting filter that provide a wavelength range between 200

and 1100 nm with optical resolution of 1,0 nm (FWHM). A 2048-element linear silicon CCD array measures the intensity of the spectrum [101]. Lambda 1050 is a high performance device featured with a PMT, InGaAs and PbS 3-detector module, which enables analyzes in wavelengths from 175 nm to 3300 nm [102]. Both analyzers have integrated software that permits data to be exported in different formats.

3.1.4 Material

For the verification of the prototype, areas of 5 x 5 mm^2 were processed in printed circuit boards. The process radiation emitted during the procedure was investigated. The PCBs used were made of copper foils of 18 µm of thickness deposited on fiber reinforced glass epoxy resin (FR-4) substrate. New boards without structures as well as boards with structured copper tracks were used.

3.2 PROTOTYPE DEVELOPMENT

In the scope of project MaLDeAN, a high speed and high sensitive sensor was developed, based on the analysis of the process radiation generated in the interaction zone of laser and workpiece, in a configuration that allowed an easy integration to the machine. The characteristics of the system must permit the local and temporal resolved observation of the process. These characteristics must meet the requirements imposed by the process parameters shown in Table 3.

Table 3 - Process parameters.

Laser output power [P]	25% (12,5 W)
Pulse width [τ_l]	6 ps
Pulse repetition rate [f_{rep}]	800 kHz
Scan speed [V_s]	2 - 4 m/s

Source: The author.

For the development of the monitoring system, activities were divided in three major parts: concept of the sensor system; implementation; and calibration & verification.

Figure 27 - Methodology for the development of the monitoring system.

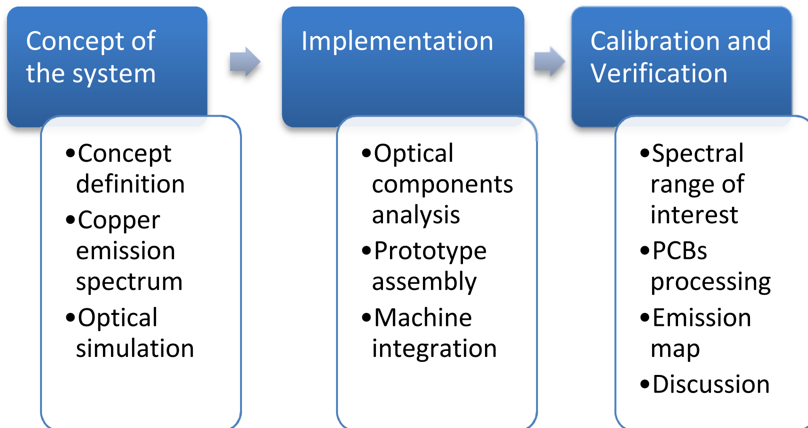

Source: The author.

Based on the optical spectrum analyzers presented in section 2.5, a concept for the system is defined. Tests with the Ocean Optics spectrometer during laser processing of copper characterize the spectrum of the process radiation. The design of the chosen optical configuration is simulated with the software Zemax®, where diverse coatings and positions for the optical components (spherical mirrors, lenses etc.) are tested. Different photodetectors are compared to select the one that best fits the process requirements.

With the definition of the optical configuration as well as of the optical components the prototype is assembled. The spectral characteristics of the ablation machine optical constituents (e.g. flat-field lens, scan head, mirrors) are analyzed for the implementation of a coaxial process monitoring strategy. Coaxial strategy is used, because it is independent of the movements of the laser beam into the working field, since the sensor always captures information from the interaction zone of laser and workpiece. The mechanical integration of the monitoring system with the machine is designed and evaluated with the software CAD Autodesk Inventor®. For the construction of the system, the limited space in the machine enclosure must be taken into account.

The assembled prototype is tuned to the spectral range of interest, according to the material processed (copper). For calibration, the Ocean

Optics spectrometer, a light bulb and calibration lamps called pen-rays, which emit radiation in a defined well-known spectrum are used. Then, the system is tested at the laser ablation machine during the processing of printed circuit boards, with the objective of identifying the presence of copper. Position information of the laser beam on the workpiece and emission data are gathered to create an emission map of the processing of each layer of material. The emission map is compared to microscope images to validate the system performance. The performance of the system is discussed.

4 CONCEPT OF THE SENSOR SYSTEM

4.1 DEFINITION OF THE CONCEPT

When materials are subjected to high temperatures they emit radiation in specific wavelengths, according to the their composition [103]. This characteristic is explored to analyze the process radiation emitted during laser ablation of printed circuit boards.

PCBs are basically made of copper foils deposited on FR-4 substrate. In the processing (e.g. in the direct structuring of circuit layouts), unwanted copper layer is removed by the interaction of the material with the laser beam. Minimum damage in the substrate is wanted. To monitor the process, the characteristic radiation spectrum emitted during the ablation of copper was observed. When the emission spectrum changes for different wavelengths, it is considered that the copper layer is completely removed and the FR-4 layer is interacting with the laser. The monitoring system may contribute to the quality of the process as well as reduce processing time, considering that it will display the state of the conductive layer subjected to ablation and also show when it is completely removed. At the same time regions without copper will not be ablated more than needed, avoiding damages in the substrate.

This analysis can be performed using a high-speed and high sensitive spectrometer. Since standard spectrometers hardly combine the response time and sensitivity required by the process parameters, an optical spectrum analyzer with fast response time and high sensitivity was developed. The system is based on the diffraction grating optical spectrum analyzer architecture, because it presents good wavelength separation, leading to high performance in terms of resolution, along with good sensitivity. The optical bench based on a monochromator in the Czerny-Turner configuration shows to be a feasible choice, as it can be assembled in a compact space inside the ablation machine and it involves standard components available in the market in viable prices.

Figure 28 - Concept of the monitoring system.

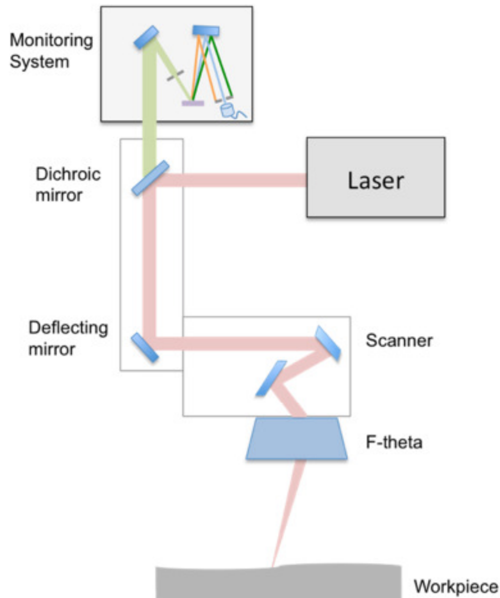

Source: The author.

Considering the process speed and low levels of radiation intensity produced by picosecond laser pulses, a fast and high sensitive photodetector must be employed. As array detectors analyze simultaneously a wide part of the spectrum, they show a limitation for reaching fast enough response times required by the process. An alternative to overcome this limitation is to monitor only a small range of wavelengths, that is part of the copper emission spectrum. In this case ultrafast single detectors become suitable for time resolved observations. Additionally, when integrated with the machine the detector is exposed to the laser ablation environment. For this reason, besides being fast and high sensitive, it must be robust.

To define the most suitable photodetector it is important to know the copper emission spectrum. This information is essential in order to choose a detector that has high efficiency in the wavelength region of interest. To determine the copper emission spectrum, the process radiation was recorded by the Ocean Optics spectrometer during the laser ablation of PCBs. The spectrometer was assembled in a coaxial

configuration through a dichroic mirror that allows wavelengths between 400 and 900 nm to pass to the detector. A spherical mirror was responsible for focusing the radiation onto the spectrometer fiber input. Figure 29 exhibits the copper emission spectrum for spectrometer integration times of 1 s, 2 s and 3 s, during laser processing with P = 12,5 W, V_s = 4 m/s and f_{rep} = 800 kHz. The dark spectrum, i.e. detector's background signal even when there is no incident light, was subtracted of each curve. Besides other small peaks, the chart shows 3 well-distinguished spectral lines at 510 nm, 514 nm and 521 nm, which represent the copper emission. The wavelength region from 510 to 521 nm is used in the development of the monitoring system. The peak at 1030 nm comes from the small amount of radiation from the processing laser that passes through the dichroic mirror (the dichroic mirror does not reflect 100% of the laser light).

Figure 29 - Copper emission spectrum for spectrometer integration times of 1 s, 2 s and 3 s, during laser processing. Dark spectrum is subtracted.

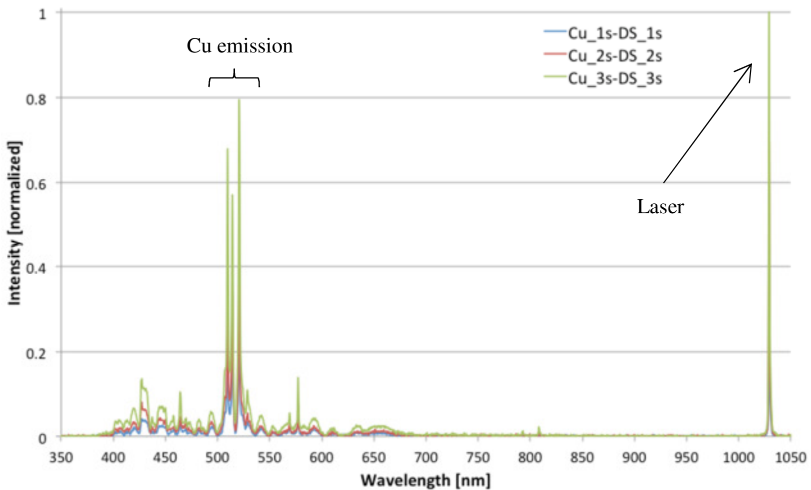

Source: The author.

In the same assembly, substrate material FR-4 was subjected to laser ablation with the same process parameters and the emission spectrum was recorded. Then, the spectrum of FR-4 and copper were compared in order to assure that they did not have coincident lines in the emitted spectrum. Figure 30 shows the comparison of copper (blue line)

and FR-4 (red line) spectrum. The peaks at the wavelengths of 510, 514 and 521 are characteristics of copper.

Figure 30 – Comparison of copper and FR-4 emission spectrum for 1 s integration time. Dark spectrum is subtracted.

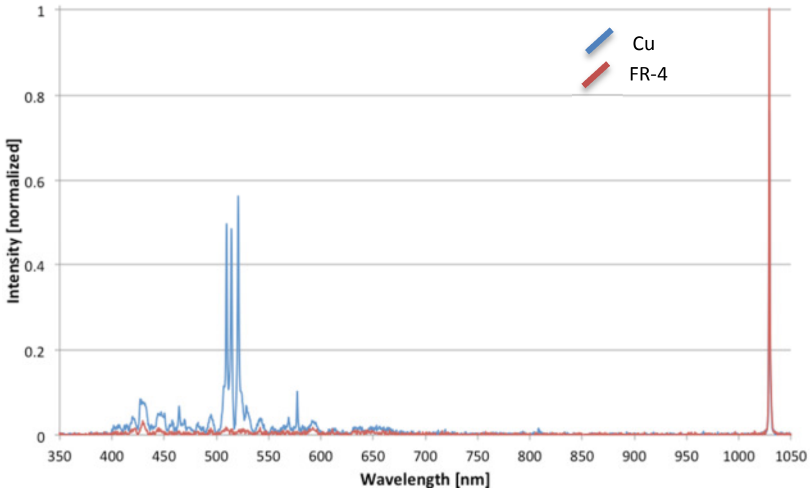

Source: The author.

With the spectral region of interest for the monitoring system defined, it was possible to choose a suitable detector. Various detector technologies were compared. Photomultiplier tubes are stable and have low noise, but they are bulky, delicate and need costly high voltage power supplies. PIN photodiodes do not have these drawbacks. Instead they have a complete lack of internal gain. Avalanche photodiodes present high photon detection efficiency (PDE), compact size and ruggedness, but also excess noise [98]. Silicon photomultipliers, along with compactness, ruggedness and magnetic insensitivity, have high gain with low bias voltage and low noise, showing to be the most appropriated detector for the application. Table 4 shows a detailed comparison of different detector technologies. It is possible to note that silicon photomultipliers presents the desired characteristics for the prototype detector.

Table 4 - Comparison of various detector technologies.

	PIN	APD	PMT	SPM
Gain	1	10^2	10^6	10^6
Operational Bias	Low	High	High	Low**
Temp. sensitivity	Low	High	Low	Low
Mechanical robustness	High	Medium	Low	High
Ambient light exposure?	OK	OK	No	OK
Spectral range	Red	Red	Blue/UV	Green
Readout / Electronics	Complex	Complex	Simple	Simple
Form factor	Compact	Compact	Bulky	Compact
Large area available?	No	No	Yes	Yes
Sensitive to magnetic fields?	Yes*	Yes*	Yes	No
Noise	Low	Medium	Low	High
Rise time	Medium	Slow	Fast	Fast

* Due to the requirement for the external electronics to be located close to the detector.
**SPM from SensL, having an operational bias of 30V, meet the requirements of the Extra Low Voltage directive.

Source: [98].

For this reason, a SensL MiniSL silicon photomultiplier module was employed. It is a high-performance detector module, which consists of a SPM detector with spectral range from 400 to 1000 nm and peak wavelength at 500 nm. Cooling is available using a Peltier thermoelectric cooler. The photon detection efficiency is shown in Figure 31. Technical specifications are found in Attachment A.

Figure 31 - SensL Mini SL photon detection efficiency.

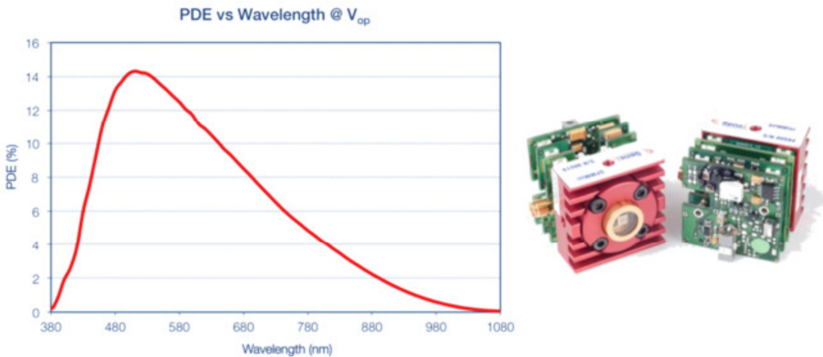

Source: SensL.

4.2 OPTICAL SIMULATION

The objective of the system is to separate the spectrum of the emitted radiation in narrow wavelength ranges and analyze a specific spectral region. For this, an optical bench based on a monochromator with the Czerny-Turner configuration was designed. As mentioned before, this configuration involves two spherical (concave) mirrors and a diffraction grating.

The optical arrangement was defined using the software for optical simulation Zemax®. In the simulation, different angles of adjustment, distances between components and mirrors with distinct focal lengths and sizes were tested. These changes in the design were directly connected to the resolution of the system.

In a coaxial monitoring strategy, radiation emitted from the process travels through the f-theta lens, where it is collimated. After that, the collimated radiation meets the scanner moving mirrors, a deflecting mirror and a dichroic mirror until it reaches the coaxial-integrated optical spectrum analyzer. Then, the process radiation is focused on a mechanical slit, by a 1" spherical mirror. The slit selects part of the image to go through its aperture and to meet a 2" spherical mirror. This mirror collimates the beam and directs it to the diffraction grating. The diffraction is only controlled if the light is collimated. On the diffraction grating the reflected light is separated in narrow wavelength ranges, which travel collimated until the next 2" spherical

mirror. This mirror focuses each wavelength range on the second mechanical slit, before the radiation reaches the detector surface.

Figure 32 shows a detail of the simulated optical layout. Different wavelengths are separated in the detector plane. The second slit and the detector are not displayed. The complete design is available in Appendix A.

Figure 32 - Detail of the optical layout.

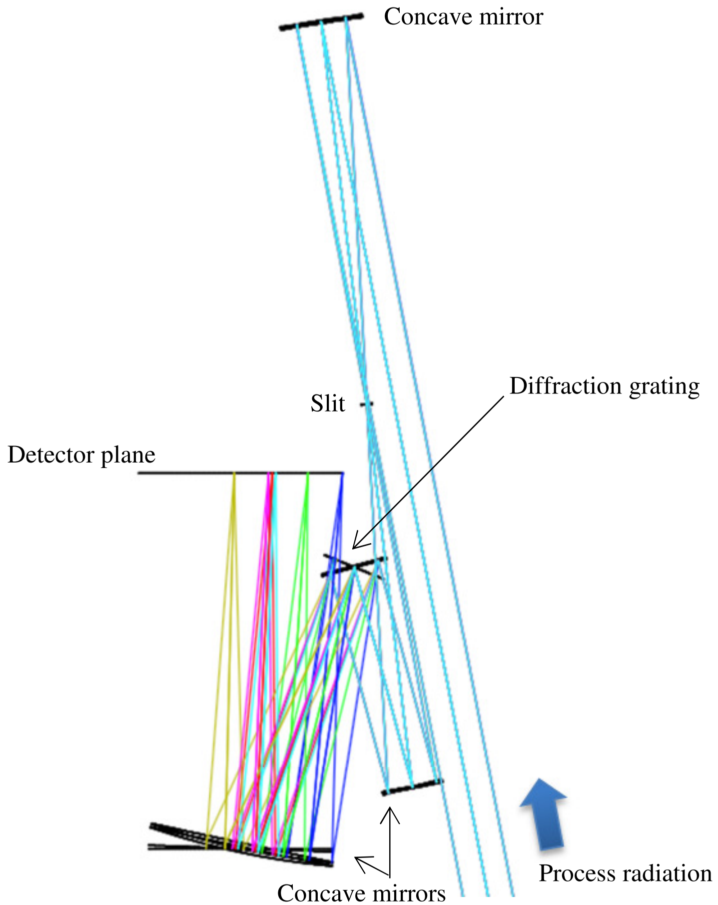

Source: The author.

The slits play an important role in the optical resolution and throughput of the system. Without the entrance slit, a complete object would be imaged for each separated wavelength range in the sensor plane, causing images overlap. So, the entrance slit defines a clear-cut object for the optical bench [104]. The exit slit selects the wavelengths that may pass through the aperture and achieve the detector. Narrow slit widths lead to more optical resolution, whereas fewer throughputs, since less intensity of light reach the detector.

Using spherical mirrors instead of lenses may avoid resolutions losses caused by the different angles of refraction of different wavelengths, when light passes through the lens material. As the spherical mirror reflects the radiation, it focuses the polychromatic light components at the same point.

By rotating the diffraction grating it is possible to select different wavelengths to reach the detector. The rotation of the grating changes the direction of the reflected light. Consequently, the spherical mirror focuses different wavelengths on the slit aperture, allowing the analysis of another spectral band.

In the simulation it was noticed that the intensity of the image in the detector plane decreases as the angles of direction of the mirrors in relation of the optical path increase. But if the angles are too small, the grating diffracts the light on the collimating spherical mirror and the mirror reflects it back to the first slit.

5 IMPLEMENTATION OF THE SENSOR SYSTEM

With a defined conception of the system and a simulated design, it was possible to assembly the prototype and to integrate it with the laser ablation machine. In the next sections the elements of the system, the assembly and the machine integration are described.

5.1 CHARACTERIZATION OF THE OPTICAL COMPONENTS

5.1.1 Monitoring System Components and Assembly

During the optical simulation, measurements were performed at the machine, aiming to verify if there was enough space for an optical assembly. Since the area where the laser interacted to the workpiece was secluded from the external environment by a door, the machine had a limited space for build up the analysis system. Therefore, a plane high-reflective mirror was responsible for deflecting the process radiation 90° from the original axis to an area where the assembly was possible. After the deflection, the radiation met a spherical mirror and it was focused on the entrance slit aperture to interact with the optical components of the system until it reached the detector. Table 5 shows the specifications of the optical elements used in the assembly.

Table 5 - Optical components specifications.

Component	Dimensions [mm]	Coating spec.	Other spec.
Plane mirror	Ø 25,4	RAL UV	Flatness λ/10
Shortpass Filter 775 nm	Ø 25,0	Hard dielectric sputtered	OD > 4
Spherical mirror	Ø 25,4	UV enhanced Al (R @ 250 - 700 nm)	f = 101,6 mm
Spherical mirror (2x)	Ø 50,8	UV enhanced Al (R @ 250 - 700 nm)	f = 101,6 mm
Diffraction grating	30 x 30	Bare Gold/NIR (700 - 1100 nm); blaze λ: 800 nm	830 gr./mm; Ruled
Slits (2x)	0 – 6	-	µm adjustable

Source: The author.

All mirrors were designed for high efficiency in a spectral bandwidth that encompasses the wavelength range of interest. The efficiency of the diffraction grating used was optimized for 800 nm. It was an element already available at Fraunhofer ILT and showed acceptable results in separating the optical spectrum at the wavelengths observed. Its typical efficiency curve is available in Attachment B.

The optical arrangement was constructed on an aluminum breadboard (platform for assembling prototype optical assemblies) of 250 x 300 mm with an aperture. Mechanical adaptations to the machine integration will be detailed in the next section. Accessories for optical assembly were used to build the prototype. The plane mirror was fixed at 45º to the optical path in a right angle kinetic mount. Rods connected the right angle kinetic mount to a filter cage plate. The Ø 25,4 mm mirror was assembled in a cage assembly Turret mount, which allowed direction adjustments in the horizontal and in the vertical planes. The Ø 50,8 mm mirrors were mounted in lens mount tubes. Posts and post holders with variable height guaranteed the vertical alignment of all components, except for the grating. The latter was set at a holder in a continuous rotation stage with adjustable angle, fixed on a platform with controlled elevation. The adjustable rotation stage permitted variations in the angle direction of the grating and, consequently, in the wavelength tuning of the system.

Figure 33 presents the prototype assembly on the breadboard. The numbered components are: 1) plane mirror; 2) short pass filter; 3) Ø 25,4 mm spherical mirror; 4) entrance slit 5) Ø 50,8 mm spherical (collimating) mirror; 6) diffraction grating; 7) Ø 50,8 mm spherical (focusing) mirror; 8) exit slit. An optic fiber connected to the exit slit takes the light to the detector.

Figure 33 - Prototype assembly.

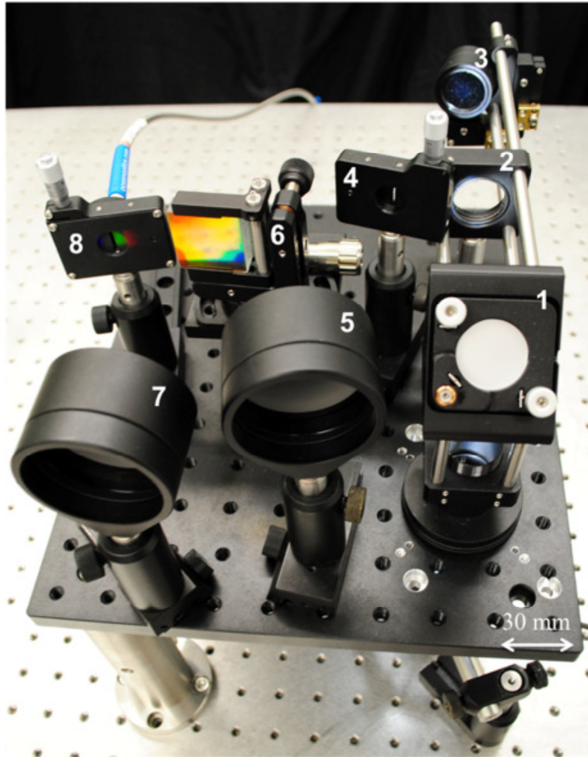

Source: The author.

5.1.2 LT 50 Components

Before reaching the monitoring system, the process radiation passed through some of the laser ablation machine optical components, such as the f-theta lens, the scanner moving mirrors, a deflecting mirror and a dichroic mirror (see Figure 28). The optical characteristics of these elements influenced the result of the analysis. In order to have satisfactory results, the LT 50 components must permit the radiation in the spectral region of interest (from 510 to 521 nm) to achieve the detector.

Two f-theta lenses were available for the process: a Rodenstock and a Sill color-corrected lens, both with focal length of 163 mm. Color-

corrected lenses have the same focal length and working distance for the designed wavelengths, resulting in identical image fields and avoiding chromatic aberrations [105]. Transmission measurements were carried out with the Perkin Elmer Lambda 1050 spectrophotometer for comparison of the two lenses (Figure 34).

Figure 34 - Transmission measurements of Rodenstock (red line) and Sill color-corrected (blue line) f-theta lenses. Both curves are normalized to their maximum values.

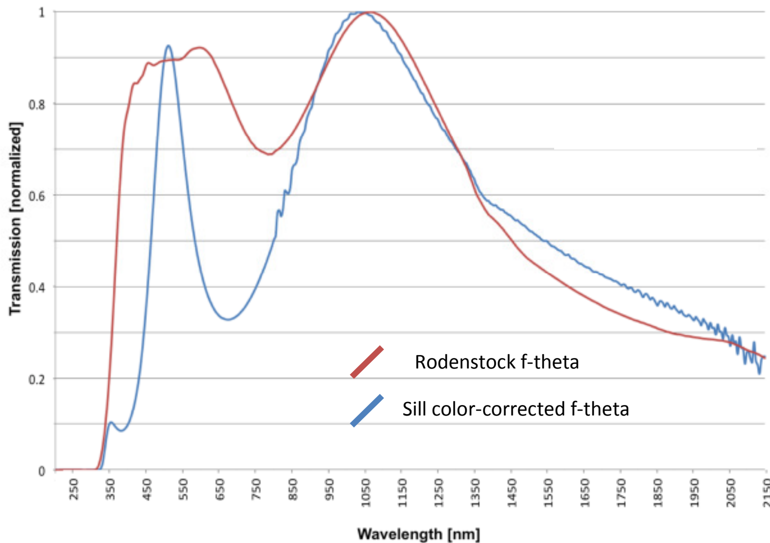

Source: The author.

Sill f-theta has the advantage of being color corrected for 532 nm and 1064 nm and designed for ultrashort pulse applications, but it exhibited a narrow peak at 565 nm and presented less transmission in the wavelengths chosen for monitoring. For this reason, even not being color-corrected, the Rodenstock f-theta was chosen to test the prototype.

Regarding the scan head, the machine was originally integrated with a SCANLAB intelliSCAN 14. It is a scanner with feedback function that contributes to dynamic performance and marking quality. IntelliSCAN 14 mirrors were designed to have high reflection at two wavelengths: 1064 nm and 800 nm. Therefore, they were not suitable for the process monitoring system, since they do not encompass the

observed spectral range. Another option available at Fraunhofer ILT was a SCABLAB hurrySCAN 20 with silver mirrors, designed for high reflection in a large spectral range, from 450 to 2500 nm. As drawback, the scanner did not have the intelliSCAN feedback function, leading to less accurate positioning. Even presenting this drawback, the optical characteristics of the hurrySCAN 20 were more adequate for the process monitoring and the hurrySCAN 20 was employed.

Other two mirrors in the optical path between the machine and the prototype were selected to permit observations of the process: a deflecting and a dichroic mirror. The former one directs the laser radiation to the process as well as the process radiation to the sensor. It must reflect as much light as possible. For this reason, a silver mirror was chosen. The mirror showed high reflectivity over a broad spectral range, fitting to the process needs (Figure 35). In the spectral range of interest, especially, the mirror reflected more than 94% of the incident radiation.

Figure 35 - Spectral analysis of the deflecting mirror.

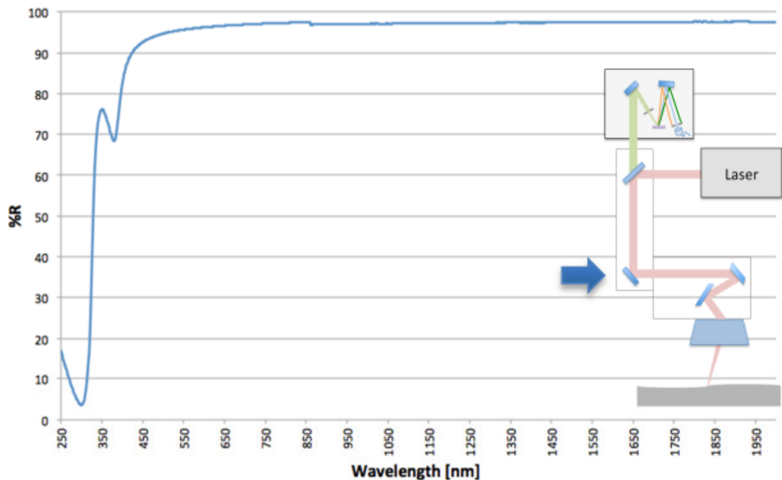

Source: The author.

The latter must reflect the laser radiation and transmit the spectral region of interest for observations. A dichroic mirror with high reflectivity between 1000 nm and 1200 nm as well as high transmittance from 400 to 900 nm and from 1200 to 1900 nm was selected. This

mirror was responsible for the optical integration of the monitoring system with the machine. The reflectivity of the dichroic mirror (Figure 36) was measured at the Perkin Elmer Lambda 1050 spectrophotometer.

Figure 36 – Spectral analysis of the dichroic mirror.

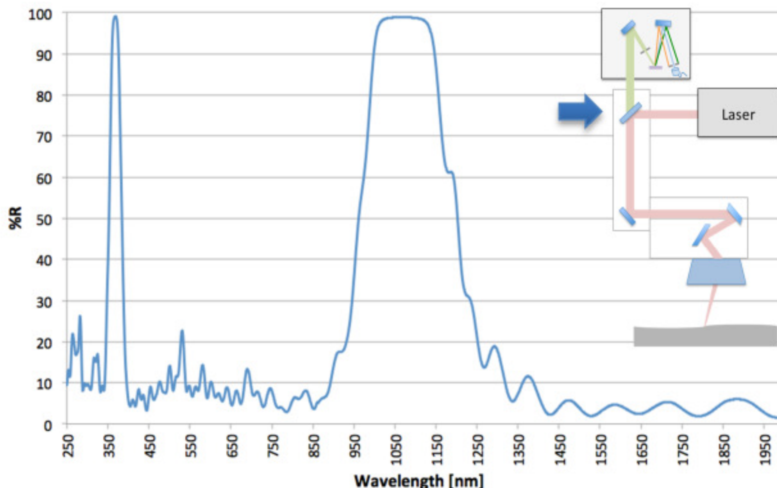

Source: The author.

The chosen components showed to be suitable for the optical integration of the monitoring system with the laser ablation machine, allowing a broad wavelength range of the process radiation to reach the detector for analysis.

5.2 MACHINE INTEGRATION

5.2.1 Mechanical Integration

The mechanical integration of the prototype with the laser ablation machine was designed with the software CAD Autodesk Inventor®. A breadboard was used as a platform for the assembly of the optical components. In the breadboard, adaptations were made to connect the platform to the machine. An aperture was drilled for the process radiation to enter in the monitoring system after passing through the dichroic mirror. To facilitate the integration with other components (e.g. the deflecting mirror), a SM2 (2,035”-40) thread was machined in

the aperture. Four through holes for M5 screws were drilled to integrate the breadboard to the LT 50.

As mentioned before, measurements were performed at the machine to evaluate the available space to assembly the prototype. As the machine door imposes limitations to the height of the system, a deflecting mirror was used to lead the construction to another direction. Figure 37 exhibits the adaptations on the breadboard for mechanical integration.

Figure 37 - Adaptations on the breadboard for mechanical integration.

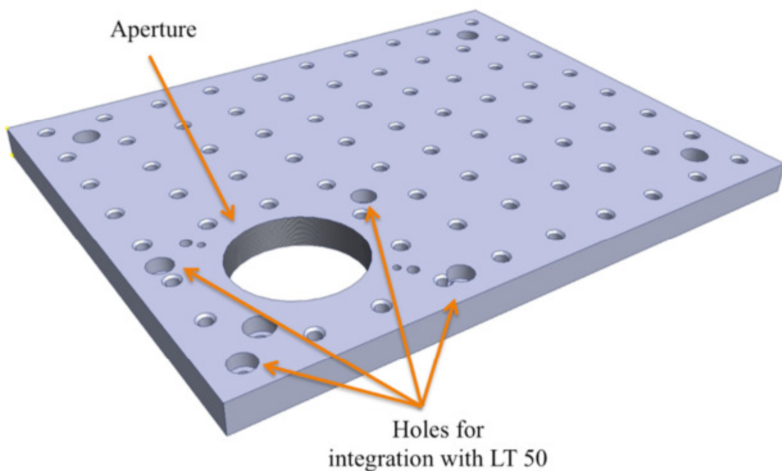

Source: The author.

To use the hurrySCAN 20 and the Rodenstock f-theta at the LT 50 it was necessary an assembly kit with adapter ring in order to connect both elements. The assembly kit available was not designed for the Rodenstock f-theta, but it guaranteed a safe connection.

5.2.2 Control Interface

The 2D scanner and the laser were controlled by the RTC5 control board from the company SCANLAB. The board also permits the integration and control of a varioSCAN, used with the intelliSCAN 14 in the original machine configuration as well as the communication with peripheral equipment.

Figure 38 - RTC5 control interface.

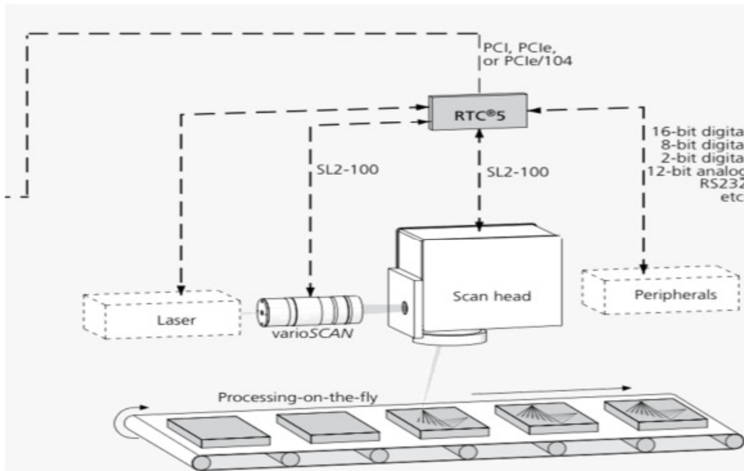

Source: Adapted from SCANLAB AG.

RTC®5 board presents feedback information for real-time monitoring. The scan system control allows reading back actual-position values [x(t), y(t)] of the 2D-scanner.

The data analysis system was developed at the Fraunhofer ILT. The analog signal from the photomultiplier is converted by an analog-digital converter (AD-converter) with a rate of 100 kHz. Simultaneously, position information from the scanner is read. A field-programmable gate array (FPGA) integrated circuit synchronizes the position data and the emission data, creating in every 10 µs a data set with intensity signal and correspondent position coordinates. Figure 39 exhibits a block diagram of the data analysis system.

Figure 39 - Block diagram of the data analysis system.

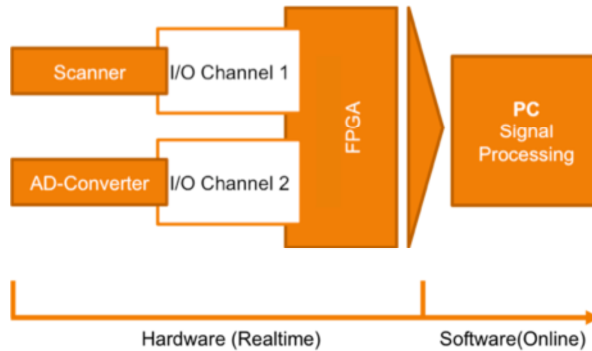

Source: Fraunhofer ILT.

From the data set a three-dimensional graph is created in the software "CPC Emission Map", developed by Fraunhofer ILT. The graph represents the process emission along the processed area. The emission map is showed in the chapter 6.2.

6 CALIBRATION AND VERIFICATION

6.1 RESOLUTION AND CALIBRATION OF THE SYSTEM

The ability of the prototype to display two signals closely spaced in wavelength as two distinct responses is determined by the wavelength resolution [67]. To determine the resolution of the system a neon pen ray line source (Figure 40) was used. Pen rays line sources are usually employed in the calibration of monochromators and spectrographs. They produce narrow, intense and well-known spectral lines from the excitation of various rare gas and metal vapors [106]. Tests for resolution were performed at the CPC laboratory, with the system separated of the LT 50.

Figure 40 - Pen-ray line source.

Source: [106].

A neon pen-ray LSP032 line source was placed at the aperture of the system. The emission spectrum was first recorded with the Ocean Optics spectrometer (Figure 41-a). At this configuration the exit slit was wide opened and a broad range of wavelengths was able to enter in the optic fiber reaching the detector. In a second configuration, the exit slit was removed and the spectrum was captured with a Nikon D3000 digital camera focused on the detector plane. To determine the image scale the camera was kept in the same position. A millimeter paper was placed in the detector plane and a picture was taken (Figure 41-b). The ratio of image pixels to 1 mm of paper revealed a scale of 99,5 px/mm.

Figure 41 - Determination of the system resolution.

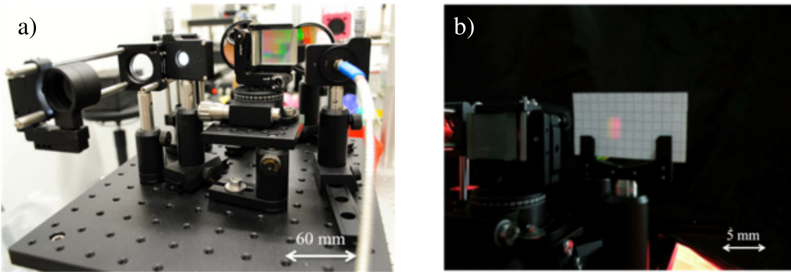

Source: The author.

The lines captured with the digital camera were compared with the intensity lines recorded with the spectrometer. This comparison is showed in Figure 42. Some lines are not displayed in the camera image, since they were out of the spectral bandwidth chosen by turning the diffraction grating.

Figure 42 - Image of part of the neon pen-ray LSP032 line source spectrum

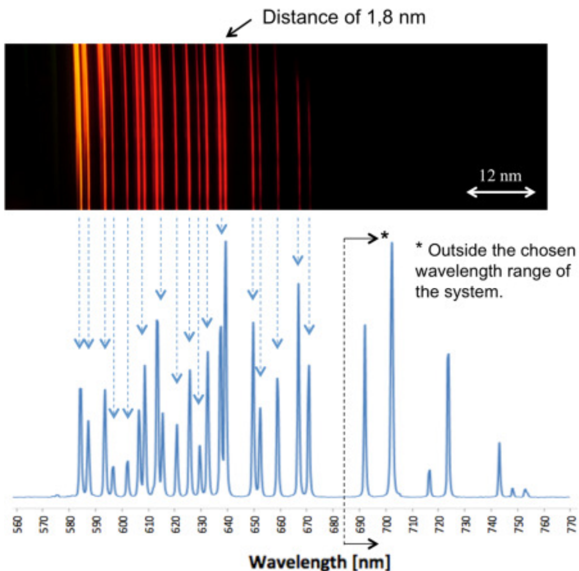

Source: The author.

With the image scale it was possible to determine spectral bandwidth in one millimeter by measuring the number of pixels separating two spectral lines.

$$\frac{\Delta\lambda}{\Delta x} = \frac{(593,7 - 587,4)x99,5}{54,72} = 11,5\ nm/mm \qquad (6.1)$$

The prototype was able to distinguish different signals spaced less than 1,8 nm from each other. It presented a good resolution for the process monitoring application.

To align the system components in the optical axis, the monitoring system was mounted in the laser ablation machine. A small light bulb secluded in an aluminum enclosure with a 1 mm hole was used. With the help of the machine positioning system (CCD camera), the 1 mm aperture was placed in the center of the working field and the light was turned on. The components were aligned in order to display the highest intensity signal in the spectrometer, meaning that the optical axis was meeting the small aperture.

Figure 43 - Alignment of the optical components.

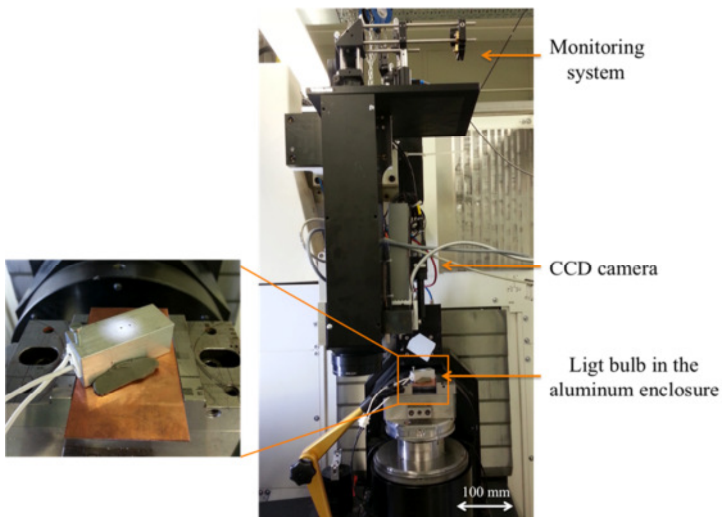

Source: The author.

For the calibration, the system was configured with the Ocean Optics spectrometer connected to the exit slit through the optic fiber. The aperture of the entrance and the exit slit was set to approx. 300 µm. The small light bulb (without enclosure) was placed in the center of the working field, irradiating light to the system. The angle of direction of the diffraction grating was changed until the spectrometer displayed a peak, where the full width at half maximum comprised wavelengths from 510 to 521 nm (Figure 44).

Figure 44 - Prototype calibration.

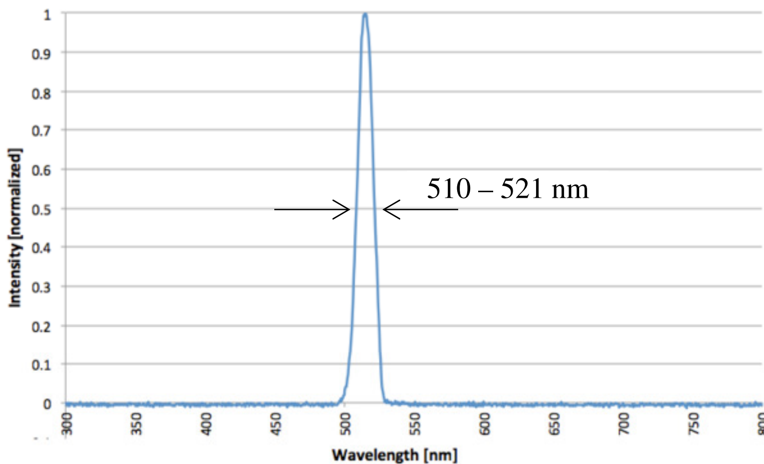

Source: The author.

6.2 VERIFICATION

After calibration the silicon photomultiplier detector was assembled with the optical arrangement. Because of the high sensitivity of the SPD, aiming to avoid interferences from other radiation sources (e.g. room light) the monitoring system was isolated in a box made of matte black aluminum foil.

Figure 45 - Monitoring system assembled in the machine.

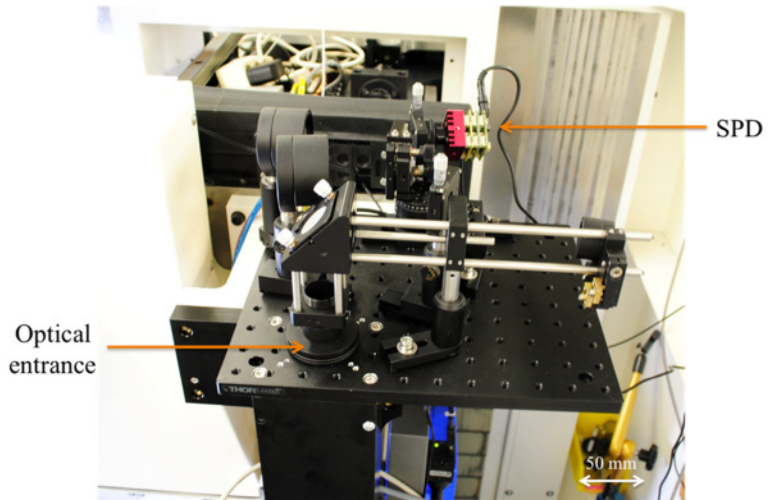

Source: The author.

Figure 46 - Prototype isolated in a matte black aluminum box.

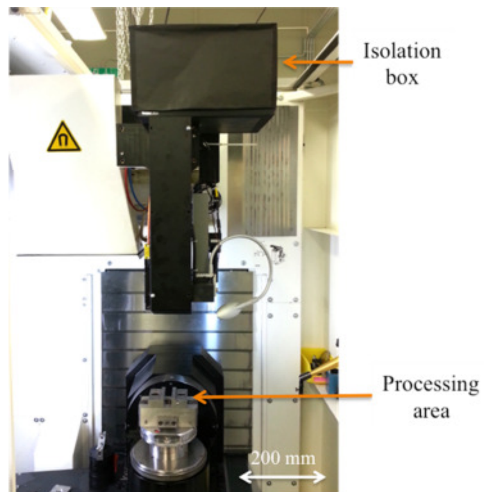

Source: The author.

Tests were carried out varying aperture widths of the entrance and the exit slit (300 µm, 600 µm, 1000 µm, 1500 µm and 2000 µm). As the slit width increased, on one hand more signal reached the detector and the system became more tolerant to misalignment. On the other hand slits wide opened showed unclear signals due to the lack of resolution. Satisfactory results were achieved with both slits width set to 1000 µm.

To verify the performance of the monitoring system, the process emission was recorded during the ablation of printed circuit boards. In a first experiment PCBs already structured, but without solder resist mask were used as samples. One layer in an area of 5 x 5 mm^2 in the center of the working field was ablated and the emission map was displayed in the software (Figure 47, right column). In the three-dimensional graph, a color matrix represents different emission intensities, characterizing the presence or absence of copper. Pictures of the processed area were taken to verify the copper recognition (Figure 47, left column).

Figure 47 - Recognition of copper tracks. P = 12,5 W; V_s = 2 m/s.

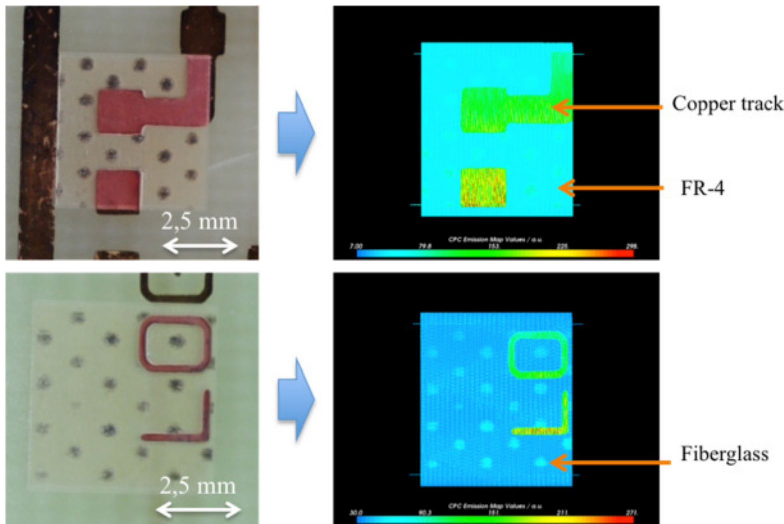

Source: The author.

The prototype was able to identify the copper emission information and, therefore, distinguish copper from FR-4. The small

spots in the map came from the crossing of glass fiber reinforcement in the fiberglass.

A second experiment was performed aiming to observe the progress of the laser ablation along different layers. After 15 layers, the process emission of each subsequent layer was recorded. The first 15 layers were not recorded to save computer space and processing efforts. They correspond to the beginning of the copper film and do not bring valuable information about the interface of the conductive material and the substrate. Figure 48 shows the progress of ablated layers. Green characterizes copper and blue characterizes FR-4. The number on each picture represents the layer being processed.

Figure 48 - Progress of ablated layers. P = 12,5 W; V_s = 2 m/s.

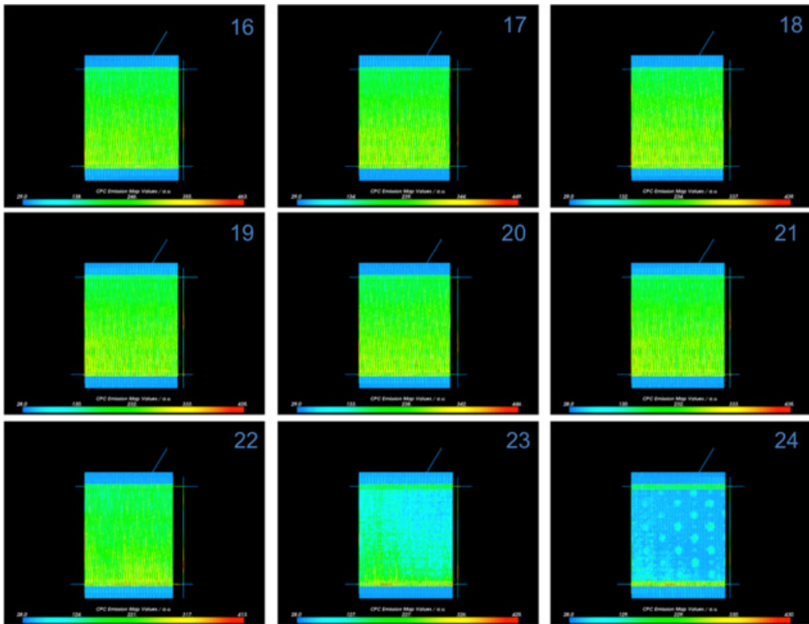

Source: The author.

It is possible to notice that copper begins to disappear in layer 23 and it is practically removed in layer 24. A microscope picture was taken after processing layer 24. Comparing the microscope picture with the emission map (Figure 49), it is observed that remaining copper in the bottom left corner was removed after this layer. Attention must be paid

when analyzing details, since the information displayed in the emission map may be similar, but not necessarily equal to the result of the ablation process. The emission map shows what happened to the material in the processing of the previous layer and not the present state of it.

Figure 49 – Comparison of microscope picture detail and emission map.

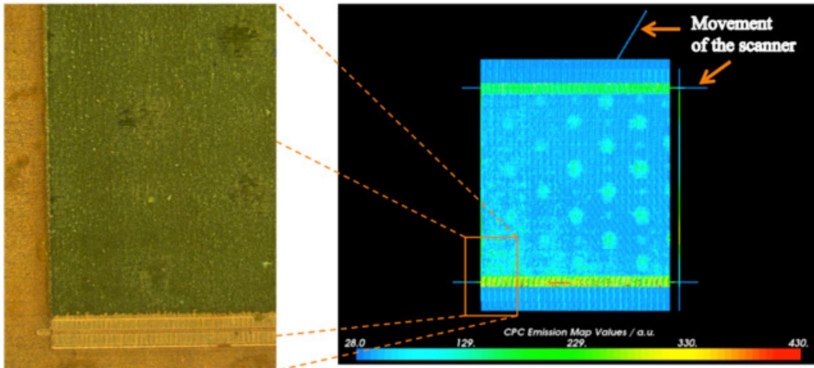

Source: The author.

The emission map in Figure 49 also reveals an irregular ablation rate, depending on the position of the processed zone in the working field. Copper on the right side of the ablated area was completely removed, while on the left side, especially in the bottom left corner, conductive material remained. It may be caused by the f-theta assembly kit, since it was not designed for the employed lens. The assembly kit guaranteed a safe connection, but not a perfect alignment between the lens and the working field plane. This misalignment may have varied the focal length, leading to a focus shift and resulting in different ablation rates. The blue lines on the top and on the sides of the emission map come from the movements of the scanner from the stand-by position to the processing area. To reduce irregular ablation rates in this experiment, the processed area was not in the center of the working field.

This issue also appeared in other samples, as presented in Figure 50. Regardless of irregular ablation rates, details could be recognized, validating the adequate resolution of the prototype. The use of the hurrySCAN 20 introduced a lack of position accuracy. Its big mirrors

with high inertia and the absence of a feedback function led to high mirror drift and delays when changing the scanning direction. At higher speeds this problem became more critical, as shown in Figure 51.

Figure 50 - Details recognition and mirror drift. Layer 24; P = 12,5 W; V_s = 2 m/s.

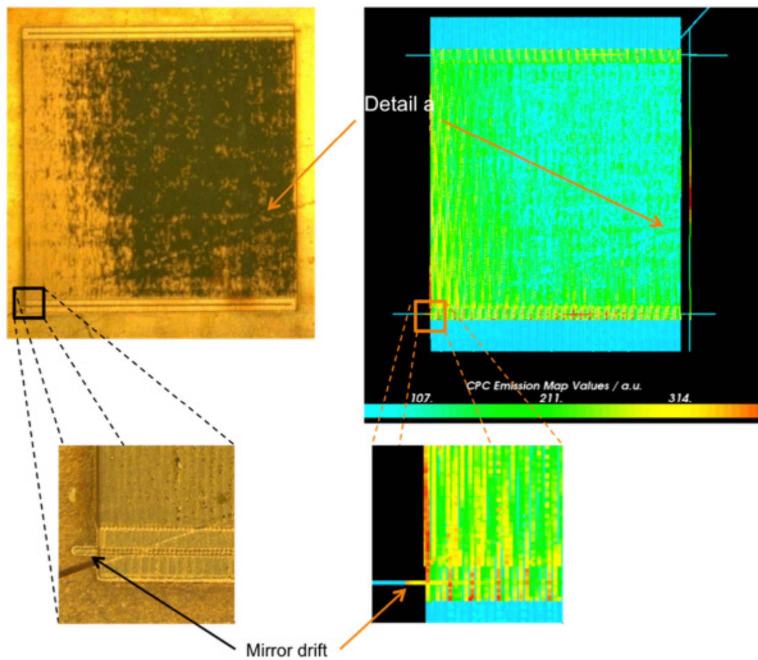

Source: The author.

Figure 51 - Low accuracy of scanner in high speeds. Layer 47; P = 12,5 W; V_s = 4 m/s

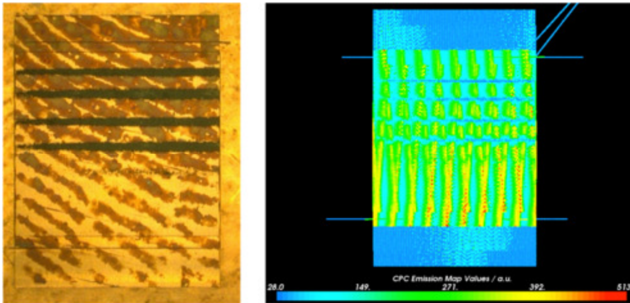

Source: The author.

At 4 m/s the result of the ablation process is influenced, demonstrating that the scanner is inadequate for such high speeds. The stains in the microscope picture are prevenient from oxidation. At 2 m/s the system already presented drifting issues, but it was still able to recognize the presence of copper layer. An additional picture showing the progress of the laser ablation process is available in Appendix B.

7 CONCLUSION

In the scope of the joint project MaLDeAN a monitoring system for the ultrashort pulse laser ablation of printed circuit boards was developed. The development process from the definition of a concept until its verification led to the following conclusions.

When ablated with a 1030 nm laser, copper emits radiation with higher intensity in a spectral range between 510 and 521 nm. Besides, the intensity of the process emission during the ablation of copper was higher than the intensity of the process emission during the ablation of the substrate material (FR-4).

The monitoring system based on a Czerny-Turner monochromator optical configuration combined with a silicon photomultiplier showed to be an adequate solution for observing the laser ablation of printed circuit boards. The better understanding of optical spectrum analyzers as well as optical simulations with different designs allowed the definition of a concept. Due to the characterization and adequacy of the LT 50 machine components the integration of the prototype was possible. The evaluation of performance verified the system's ability to detect the emitted radiation during the processing of printed circuit boards. Regions with the presence of copper could be well identified and distinguished from the areas where the conducting material was already removed. The emission map came as a valid strategy for laser ablation process monitoring. It was a direct way to show what happens to the process after each layer, contributing for a better comprehension of the involved phenomena.

The possible integration of the monitoring system with the series production could contribute to the improvement of the quality of produced parts, since regions would be continuously ablated until the complete removal of copper as well as it could collaborate to the reduction of the manufacturing time, by avoiding to keep ablating areas where copper was already removed. For this to happen, a closed-loop control software must be implemented to adequate the process parameters to the actual state of the process.

Better results could be achieved by employing a diffraction grating designed for high efficiency in a spectral bandwidth encompassing the copper emission spectral range. In addition, improvements in the system performance could be achieved using a color-corrected f-theta lens designed for the monitored wavelength range.

HurrySCAN 20 with silver mirrors presented satisfactory results in the verification of the system, but its big mirrors with high inertia among with the absence of a feedback function resulted in drifts and low position accuracy. For high precision production an intelliSCAN 14 with proper mirrors (e.g. silver mirrors) could be employed. In the same way, the f-theta assembly kit - not designed for the Rodenstock f-theta - guaranteed the connection, but did not provide an exact alignment of the lens and the working field plane, being the possible reason to irregular ablation.

7.1 SUGGESTIONS FOR FUTURE WORK

The analysis of the process emission during laser ablation of PCBs was used to develop a prototype for process monitoring. The prototype showed satisfactory results, but additional researches should be carried out to improve the system. Research topics could include:

- Investigations on irregular ablation, depending on the position in the working field. Possible reasons could be misalignments caused by the f-theta assembly kit and/or the use of a non color-corrected f-theta.
- Improvements in the system by employing a diffraction grating designed for the spectral range of interest.
- Verification of the prototype performance for laser ablation of other materials (e.g. steel). Tuning is necessary to adequate the monitoring system to the new spectrum of emitted radiation.
- Development of a closed-loop control software to adequate the process parameters (e.g. laser power, beam direction) to the actual state of the process.
- Integration of the emission map with other monitoring strategies, as optical coherence tomography, already planned in project MaLDeAN.

REFERENCES

1. SILFVAST, W. T. Lasers. In: GUENTHER, A.; PEDROTTI, L. S.; ROYCHOUDHURI, C. **Fundamentals of Photonics**. Orlando: SPIE, v. 5, 2005.

2. ERADAT, N. **Properties of Lasers**. San José: San José State University, 2009. Lecture Notes for Modern Optics.

3. STEEN, W. M.; MAZUMDER, J. **Laser Material Processing**. 4th ed. London: Springer-Verlag, 2010.

4. TRUMPF. **Laser processing with solid-state lasers**. Ditzingen: 2007.

5. BÄUERLE, D. **Laser Processing and Chemistry**. 4th ed. Heidelberg Dordrecht London New York: Springer-Verlag, 2011.

6. PASCHOTTA, R. Continuous-wave Operation. **Encyclopedia of Laser Physics and Technology**, 2008. Available at: <http://www.rp-photonics.com/continuous_wave_operation.html>. Accessed: 12/10/2014.

7. SPECTRA-PHYSICS. **Average and Peak Power – A Tutorial**. Santa Clara: Spectra-Physics - A Newport Company, v. 1, 2004. Photonics Technical Note #1: Power Meters and Detectors.

8. KORDT, J. M. **Konturnahes Laserstrahlstrukturieren für Kunststoffspritzgießwerkzeuge**. Aachen: RWTH Aachen, 2007. PhD Thesis.

9. DEUTSCHES INSTITUT FÜR NORMUNG. **DIN 8580 - Fertigungsverfahren:** Begriffe, Einleitung. Berlin: 2003.

10. O'NEILL, W. Laser Separating. In: POPRAWE, R.; WEBER, H.; HERZIGER, G. **Laser Physics and Applications**. Berlin Heidelberg New York: Springer-Verlag, v. 1, 2004.

11. DEUTSCHES INSTITUT FÜR NORMUNG. **DIN 8590 - Fertigungsverfahren Abtragen:** Einordung, Unterteilung, Begriffe. Berlin: 2003.

12. POPRAWE, R. **Lasertechnik für die Fertigung - Grundlagen,**

Perspektiven und Beispiele für den innovativen Ingenieur. Berlin Heidelberg New York: Springer-Verlag, 2005.

13. HARILAL, S. S. et al. Femtosecond Laser Ablation: Fundamentals and Applications. In: MUSAZZI, S.; PERINI, U. **Laser-Induced Breakdown Spectroscopy**. Berlin, Heidelberg: Springer-Verlag, v. 182, 2014. p. 565.

14. DEUTSCHES INSTITUT FÜR NORMUNG. **DIN 32540 - Laserstrahlabtragen - Thermisches Abtragen mit dem Laserstrahl:** Begriffe, Einflussgrößen, Durchführung. Berlin: 2012.

15. RIZVI, N. H. **Production of novel 3D microstructures using excimer laser mask projection techniques**. SPIE. Oxford: Exitech Limited. 1999.

16. GOMES, D. R. **Nanosecond ablation of alumina with an ytterbium fibre-laser:** Experimental study, topography and damage evaluation. Florianópolis: UFSC, 2014. 75 p.

17. HÜGEL, H.; DAUSINGER, F. Fundamentals of Laser-Induced Processes. In: POPRAWE, R.; WEBER, H.; HERZINGER, G. **Laser Physics and Applications**. Berlin Heidelberg New York: Springer-Verlag, v. 1, 2004.

18. BROWN, M. S.; ARNOLD, C. B. Fundamentals of Laser - Material Interaction and Application to Multiscale Surface Modification. In: SUGIOKA, K.; MEUNIER, M.; PIQUÉ, A. **Laser Precision Microfabrication**. Berlin Heidelberg New York: Springer-Verlag, 2010.

19. CHICHKOV, B. N. et al. Femtosecond, picosecond and nanosecond laser ablation of solids. **Applied Physics A**, Hannover, v. 63, n. 2, 1996.

20. PASCHOTTA, R. Fluence. **Encyclopedia of Laser Physics and Technology**, 2008. Available at: <http://www.rp-photonics.com/fluence.html?s=ak>. Accessed: 15/10/2014.

21. PASCHOTTA, R. Optical Intensity. **Encyclopedia of Laser Physics and Technology**, 2008. Available at: <http://www.rp-photonics.com/optical_intensity.html>. Accessed: 17/10/2014.

22. BYSKOV-NIELSEN, J. **Short-pulse laser ablation of metals:** Fundamentals and applications for micro-mechanical interlocking. University of Aarhus, 2010. PhD Thesis.

23. FRIEDRICH, C. Laser Ablation. **Mechanical Engineering - Michigan Technological University**, 1998. Available at: <http://www.me.mtu.edu/~microweb/chap4/ch4-2.htm>. Accessed: 18/09/2014.

24. FRAUNHOFER INSTITUTE FOR LASER TECHNOLOGY ILT. **Laser Ablation for Thin Film Structuring**. Aachen: Fraunhofer ILT, 2013. Brochure.

25. FRAUNHOFER INSTITUTE FOR LASER TECHNOLOGY ILT. **Micro and Nano Structuring with Lasers**. Aachen: Fraunhofer ILT, 2011. Brochure.

26. GEHRING GMBH & CO. KG. **Laserstrukturierung - Verbesserung der tribologischen Eigenschaften von Oberflächen**. Ostfildern: Gehring, 2007. Press release.

27. APPLIED SPECTRA. Technology: Laser Ablation. **Applied Spectra - A Laser Solutions Company**, 2014. Availbale from: <http://appliedspectra.com/technology/laser-ablation.html>. Accessed: 26/11/2014.

28. ALBAGLI, D. **Fundamental Mechanisms of Pulsed Laser Ablation of Biological Tissue**. Boston: Massachusetts Institute of Technology, 1994. PhD Thesis.

29. MATOS, A. B. et al. Laser technology for Caries Removal. In: MING-YU LI. **Contemporary Approach to Dental Caries**. Rijeka - Shanghai: Intech, 2012. p. 488.

30. SPARKFUN. PCB Basics. **Sparkfun**, 2014. Available at: <https://learn.sparkfun.com/tutorials/pcb-basics>. Accessed: 26/11/2014.

31. FORD, D. N.; CAVETTE, C. Printed Circuit Boards. **How Products Are Made**. Available at: <http://www.madehow.com/Volume-2/Printed-Circuit-Board.html>. Accessed: 26/11/2014.

32. ELECTROSOFT ENGINEERING. Concepts and terminology used in Printed Circuit Boards (PCB). **Electrosoft Engineering**, 2010. Available at: <http://www.pcb.electrosoft-engineering.com/04-articles-custom-system-design-and-pcb/01-printed-circuit-board-concepts/printed-circuit-board-pcb-concepts.html>. Accessed: 02/12/2014.

33. MEHL, E. L. D. M. Departamento de Engenharia Elétrica UFPR. **Conceitos Fundamentais sobre Placas de Circuito Impresso**. Available at: <http://www.eletrica.ufpr.br/mehl/te232/textos/PCI_Conceitos_fundamentais.pdf>. Accessed: 02/12/2014.

34. YANO, V. A. N. **Placas de Circuito Impresso - Conceitos Fundamentais**. Universidade Tecnológica Federal do Paraná. Available at: <http://paginapessoal.utfpr.edu.br/vitoryano/el06d-laboratorio-de-eletronica/pci-parte1.pdf/view>. Accessed: 02/12/2014.

35. LEWIS, H. J.; RYAN, A. **Printing as an Alternative Manufacturing Process for Printed Circuit Boards**. In: MENG JOO Er (Ed.). Printing as an Alternative Manufacturing Process for Printed Circuit Boards, New Trends in Technologies: Devices, Computer, Communication and Industrial Systems. Rijeka - Shanghai: Intech, 2010.

36. ASUNI, N. Technik.net - Electronic Hardware Information, Guides and Tools. **PCBs Fabrication Methods**, 2011. Available at: <http://www.technick.net/public/code/cp_dpage.php?aiocp_dp=guide_pcb>. Accessed: 02/12/2014.

37. YANO, V. A. N. **Placas de Circuito Impresso - Métodos de Produção**. Universidade Tecnológica Federal do Paraná. Available at: < http://paginapessoal.utfpr.edu.br/vitoryano/el06d-laboratorio-de-eletronica/pci-parte2.pdf/view>. Accessed: 02/12/2014.

38. GROOVER, M. **Fundamentals of Modern Manufacturing**. 3rd ed. New York: John Wiley & Sons, 2006.

39. LPKF LASER & ELECTRONICS AG. **In-House Rapid Prototyping**. Garbsen: LPKF Laser & Electronics AG, 2014. Product Catalog.

40. MEIER, D. J.; SCHMIDT, S. H. **PCB Laser Technology for Rigid and Flex HDI – Via Formation, Structuring, Routing**. Garbsen - Wilsonville: LPKF Laser & Electronics AG , 2002.

41. GOLD PHOENIX PRINTED CIRCUIT BOARD CO., LTD. The definition of HDI PCB. **Gold Phoenix PCB**, 2012. Available at: <http://www.goldphoenixpcb.com/html/Support_Resource/others/arc_133.html>. Accessed: 03/12/2014.

42. VENKAT, S.; HANNON, T. **Laser Processing- The Future of HDI**

Manufacturing. Electronics Manufacturing Technology Symposium. San Jose: IEEE. 2002. p. 149 - 153.

43. LPKF LASER & ELECTRONICS AG. Applications: PCB Processing - Drilling of Microvias. **LPKF Laser & Electronics**, 2014. Available at: <http://www.lpkf.com/applications/pcb-processing/drilling-microvias.htm>. Accessed: 04/12/2014.

44. LPKF LASER & ELECTRONICS AG. Applications: PCB Processing - Cutting of Multilayers. **LPKF Laser & Electronics**, 2014. Available at: <http://www.lpkf.com/applications/pcb-processing/cutting.htm>. Accessed: 04/12/2014.

45. BLATT, P. **Laser Direct Imaging Benefits from Solid State Technology**. International Conference on Laser Assisted Net Shape Engineering 5. Erlangen: Proceedings of the LANE 2007. 2007. p. 1221-1224.

46. BARBUCHA, R. et al. Laser Direct Imaging of Tracks on PCB Covered with Laser Photoresist. **Bulletin of the Polish Academy of Sciences**, Gdańsk, v. 56, n. 1, 2008.

47. LPKF LASER & ELECTRONICS AG. Applications: PCB Processing - Resist Exposure. **LPKF Laser & Electronics**, 2014. Available at: <http://www.lpkf.com/applications/pcb-processing/conductive-pattern-creation/resist-exposure.htm>. Accessed: 04/12/2014.

48. LPKF LASER & ELECTRONICS AG. Applications: PCB Processing - Resist Structuring. **LPKF Laser & Electronics**, 2014. Available at: <http://www.lpkf.com/applications/pcb-processing/conductive-pattern-creation/resist-structuring/index.htm>. Accessed: 04/12/2014.

49. LPKF LASER & ELECTRONICS AG. **Application Report:** LPKF MicroLine UV Laser Systems - Laser Removal of Chemical Tin for the Production of Ultra-fine Lines. Garbsen: LPKF Laser & Electronics AG, 2014.

50. LPKF LASER & ELECTRONICS AG. **The Next Generation of In-House Prototyping - LPKF ProtoLaser S**. Garbsen: LPKF Laser & Electronics, 2014. Product catalog.

51. LPKF LASER & ELECTRONICS AG. **The Swiss Army Knife of the Laboratory:** Micro-Material Processing with the LPKF ProtoLaser U3.

Garbsen: LPKF Laser & Electronics, 2014. Product catalog.

52. LPKF LASER & ELECTRONICS AG. Applications: Rapid PCB Prototyping - Laser Structuring of PCBs. **LPKF Laser & Electronics**, 2014. Available at: <http://www.lpkf.com/applications/rapid-pcb-prototyping/circuit-boards/laser-structuring.htm>. Accessed: 05/12/2014.

53. LASER MICRONICS GMBH. **Micromaterial Processing with Lasers:** Project Planning, Prototyping, Job-Shop Production. Garbsen: Laser Micronics, 2014. Press release.

54. LPKF LASER & ELECTRONICS AG. Applications: Laser Direct Structuring (LDS). **LPKF Laser & Electronics**, 2014. Available at: <http://www.lpkf.com/applications/mid/index.htm>. Accessed: 05/12/2014.

55. FRAUNHOFER INSTITUTE FOR LASER TECHNOLOGY ILT. **Process Control in Laser Materials Processing**. Aachen: Fraunhofer ILT, 2011. Brochure.

56. WIESEMANN, W. Process Monitoring and Closed-Loop Control. In: POPRAWE, R.; WEBER, H.; HERZINGER, G. **Laser Physics and Applications**. Berlin Heidelberg New York: Springer-Verlag, v. 1, 2004.

57. SCHMITT, R. et al. **Inline process metrology system for the control of laser surface structuring processes**. LANE 2012. Fürth: Physics Procedia 39. 2012. p. 814 - 822.

58. THORLABS. Optical Coherence Tomography Tutorial. **Thorlabs**, 2014. Available at: <http://www.thorlabs.com/newgrouppage9.cfm?objectgroup_id=5702 >. Accessed: 10/12/2014.

59. NOVACAM TECHNOLOGIES INC. Technology: How low-coherence interferometry works. **Novacam Technologies Inc.:** Profilometry & OCT Systems Worldwide, 2014. Available at: <http://www.novacam.com/technology/how-lci-works/>. Accessed: 10/12/2014.

60. TARGOWSKI, P. et al. **Picosecond laser ablation system with process control by Optical Coherence Tomography**. SPIE. Orlando: SPIE Digital Library. 2009.

61. RUSSO, R. E. Laser Ablation. **Applied Spectroscopy**, Berkeley, v. 49, n. 9, p. 14 - 28, 1995.

62. STURM, V.; PETER, L.; NOLL, R. Steel Analysis with Laser-Induced Breakdown Spectrometry in the Vacuum Ultraviolet. **Applied Spectroscopy**, Aachen, v. 54, n. 9, p. 1275 - 1278, 2000.

63. LORENZEN, C. J. et al. Applications of Laser-induced Emission Spectral Analysis for Industrial Process and Quality Control. **Journal of Analytical Atomic Spectrometry**, Essen, v. 7, p. 1029 - 1035, 1992.

64. MATEO, M. P.; CABALÍN, L. M.; LASERNA, J. Line-focused laser ablation for depth-profiling analysis of coated and layered materials. **Applied Optics**, Málaga, v. 42, n. 30, p. 6057 - 6062, 2003.

65. MARGETIC, V. et al. Depth profiling of multi-layer samples using femtosecond laser ablation. **Journal of Analytical Atomic Spectrometry**, Dortmund, v. 16, p. 616 - 621, 2001.

66. CHEN, C. H.; MCCANN, M. P.; PHILLIPS, R. C. Real-time Monitoring of Laser Ablation Deposition of Superconductors by Fluorescence and Secondary-ion Spectra. **Applied Physics Letters**, Oak Ridge, 53, n. 26, 1988. p. 2701 - 2703.

67. AGILENT TECHNOLOGIES. **Optical Spectrum Analysis**. Santa Clara: Agilent Technologies, 2000. Application Note 1550-4.

68. PASCHOTTA, R. Optical Spectrum. **Encyclopedia of Laser Physics and Technology**, 2008. Available at: <http://www.rp-photonics.com/optical_spectrum.html>. Accessed: 12/12/2014.

69. YOKOGAWA ELECTRIC CORPORATION. Products: Optical Test Equipment - Optical Spectrum Analyzer. **Yokogawa Test & Measurement**, 2014. Available at: <http://tmi.yokogawa.com/products/optical-measuring-instruments/optical-spectrum-analyzer/>. Accessed: 12/12/2014.

70. PASCHOTTA, R. Spectrometers. **Encyclopedia of Laser Physics and Technology**, 2008. Available at: <http://www.rp-photonics.com/spectrometers.html?s=ak>. Accessed: 13/12/2014.

71. PASCHOTTA, R. Interferometers. **Encyclopedia of Laser Physics and**

Technology, 2008. Available at: <http://www.rp-photonics.com/interferometers.html>. Accessed: 13/12/2014.

72. PASCHOTTA, R. Fabry-Pérot Interferometers. **Encyclopedia of Laser Physics and Technology**, 2008. Available at: <http://www.rp-photonics.com/fabry_perot_interferometers.html>. Accessed: 14/12/2014.

73. NAVE, C. R. Fabry-Pérot Interferometer. **HyperPhysics**, 2014. Available at: <http://hyperphysics.phy-astr.gsu.edu/hbase/phyopt/fabry.html>. Accessed: 14/12/2014.

74. UNIVERSITÄT SIEGEN. Lehre: Fortgeschrittenen-Praktikum: Fabry-Pérot Resonator, 2007. Available at: <http://www.physik.uni-siegen.de/quantenoptik/lehre/fpraktikum/fabry-perot.html?lang=de>. Accessed: 14/12/2014.

75. AUDET, F. Photonics Handbook: Spectrum Analysis for DWDM. **EDU.Photonics**, 2014. Available at: <http://www.photonics.com/EDU/Handbook.aspx?AID=25146>. Accessed: 14/12/2014.

76. NAVE, C. R. Michelson Interferometer. **HyperPhysics**, 2014. Available at: <http://hyperphysics.phy-astr.gsu.edu/hbase/phyopt/michel.html>. Accessed: 15/12/2014.

77. NAVE, C. R. Diffraction Grating. **HyperPhysics**, 2014. Available at: <http://hyperphysics.phy-astr.gsu.edu/hbase/phyopt/grating.html>. Accessed: 17/12/2014.

78. PALMER, C. **Diffraction Grating Handbook**. 5th ed. Rochester: Thermo RGL, 2002.

79. PASCHOTTA, R. Diffraction Gratings. **Encyclopedia of Laser Physics and Technology**, 2008. Available at: <http://www.rp-photonics.com/diffraction_gratings.html>. Accessed: 18/12/2014.

80. THORLABS. Diffraction Grating - Tutorial. **Thorlabs**, 2006. Available at: <http://www.thorlabs.com/tutorials/diffgratings.cfm>. Accessed: 18/12/2014.

81. BETZLER, K. **Grating Spectrometer**. Osnabrück: Universität Osnabrück, 2002. Fachbereich Physic. Lecture notes.

82. WINKLMAIR, D. **Monochromatoren**. München: Hochschule München, v. 5. Lecture notes.

83. UNIVERSITY OF BRITISH COLUMBIA. The Monochromator and Photomultiplier. **Physics 408:** Optics, 2013. Available at: <http://www.phas.ubc.ca/~phys408/2013_14-Phys408Website_term2//Lab/Monochromator.pdf>. Accessed: 18/12/2014.

84. SPECTRAL PRODUCTS. Products: Monochromators. **Spectral Products**, 2011. Available at: <http://www.spectralproducts.com/monochromators>. Accessed: 18/12/2014.

85. VAN BRECHT, D. **The Monochromator Bandpass Filter**. Amersfoort: Yokogawa Europe BV, 2011. Optical Spectrum Analysers. Press release.

86. LOT - QUANTUM DESIGN. **Differences between Monochromators and Spectrographs**. LOT - Quantum Design, 2014. Press release.

87. OPTOMETRICS CORPORATION. **Monochromators and Modules**. Ayer: Optometrics Corporation, 2005. Press release.

88. CARL ZEISS AG. Grating - Applications Gratings: Spectroscopy. **Zeiss**, 2014. Available at: <http://www.zeiss.com/microscopy/en_de/products/gratings/applications-gratings/Spectroscopy.html>. Accessed: 18/12/2014.

89. BRALEY, J. S. **Photo Detectors**. Kingston: The University of Rhode Island, 2008. Electrical Engineering Materials - Spring 2008. Lecture notes.

90. POON, A. (Ed.). **Photodiode Detectors**. Hong Kong: Department of Electronic and Computer Engineering - HKUST, 2011. Advanced Photonics Technologies - Lecture Material.

91. PASCHOTTA, R. Photodiodes. **Encyclopedia of Laser Physics and Technology**, 2008. Available at: <http://www.rp-photonics.com/photodiodes.html>. Accessed: 20/12/2014.

92. PASCHOTTA, R. p-i-n Photodiodes. **Encyclopedia of Laser Physics and Technology**, 2008. Available at: <http://www.rp-photonics.com/p_i_n_photodiodes.html>. Accessed: 20/12/2014.

93. WANG, W.-C. **Optical Detectors**. Seattle: Department of Mechanical Engineering - University of Washington, 2011. Lecture notes.

94. PASCHOTTA, R. Avalanche Photodiodes. **Encyclopedia of Laser Physics and Technology**, 2008. Available at: <http://www.rp-photonics.com/avalanche_photodiodes.html>. Accessed: 20/12/2014.

95. HAMAMATSU PHOTONICS K.K. **Photomultiplier Tubes - Construction and Operating Characteristics Connections to External Circuits**. Iwata: Hamamatsu Photonics K.K., 1998. Product catalog.

96. PASCHOTTA, R. Photomultipliers. **Encyclopedia of Laser Physics and Technology**, 2008. Available at: <http://www.rp-photonics.com/photomultipliers.html>. Accessed: 20/12/2014.

97. FELBER, P. **Charged-coupled Devices**. Chicago: Illinois Institute of Technology, 2002. Literature study for Electrical and Computer Engineering.

98. SENSL. **Introduction to the SPM**. SensL Sense Light, v. 3.1, 2011. Technical Note.

99. DMG MORI. **LASERTEC Series**. Dübendorf: Montfort Werbung, 2014. Product Catalog.

100. TRUMPF. **TruMicro:** Power meets precision. Ditzingen: TRUMPF Laser- und Systemtechnik GmbH, 2014. Product Catalog.

101. OCEAN OPTICS. **HR2000 and HR2000CG-UV-NIR Series:** High-Resolution Fiber Optic Spectrometers. Dunedin: Ocean Optics, Inc., 2008. Installation and Operation Manual.

102. PERKIN ELMER. **LAMBDA UV/Vis and UV/Vis/NIR Spectrophotometers**. Waltham: Perkin Elmer, Inc., 2012. Product catalog.

103. RULISON, M. Light (Part 2) - Lecture Notes. **Dr. Rulison's Academic Homepage**, 2014. Available at: <http://www.oglethorpe.edu/faculty/~m_rulison/Astronomy/Chap%2004/chapter_4_lecture_notes.htm>. Accessed: 05/01/2015.

104. BW TEK INC. Spectrometer Knowledge. **BW Tek Inc. - Your Spectroscopy Partner**, 2014. Available at:

<http://bwtek.com/spectrometer-part-1-the-slit/>. Accessed: 05/01/2015.

105. SILL OPTICS. **Color-corrected f-theta lenses**. Wendelstein: Sill Optics, 2012. Laser Optics: F-theta. Product Catalog.

106. LOT - QUANTUM DESIGN. **Pen-Ray line sources for wavelength calibration:**. Darmstadt: LOT - Quantum Design, 2015. Product catalog.

APPENDIX A – MONITORING SYSTEM OPTICAL LAYOUT

Figure 52 - Optical layout simulated with the software Zemax.

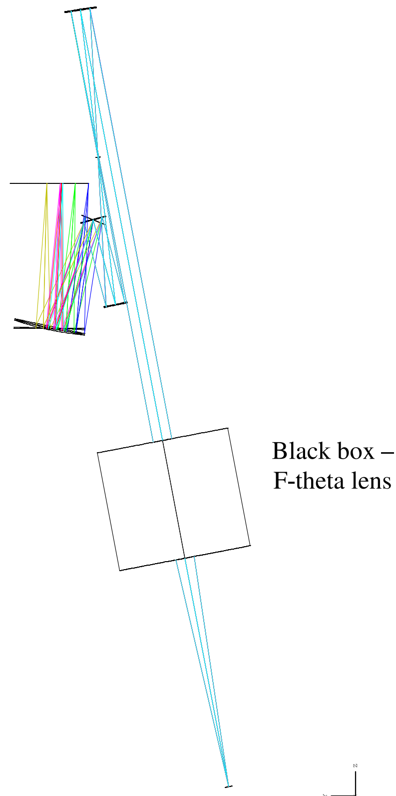

Source: The author.

APPENDIX B – PROGRESS OF LASER ABLATION PROCESS

Figure 53 – Progress of laser ablation process. P = 12,5 W; V_s = 2 m/s.

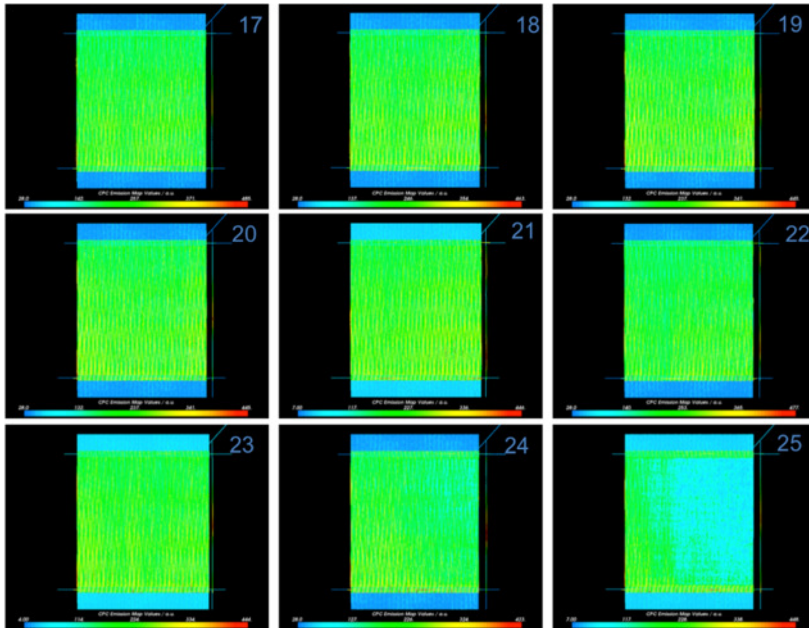

Source: The author.

ATTACHMENT A – SENSL PERFORMANCE PARAMETERS

Figure 54 - Sensl 30035 performance parameters.

	10000 series	30000 series
	10035*	30035*
Factory Set Operating Voltage (V_{op})	28.5V	
Spectral Range	400 – 1000nm	
Peak wavelength (λ_p)	500nm	
PDE at λ_p[¶]	14% ▲	
Gain	2.4×10^6 ▲	
Dark Count Rate[§]	24kHz	-
Dark Current[§]	0.013μA	0.113μA
Microcell Recovery Time	130ns ▲	130ns ▲
Cross-talk (charge duplication probability)**	21%▲	
Excess Noise Factor***	1.2▲	

[§] Measured at V_{op} with temperature reduction of ΔT.
[¶] Includes the effects of crosstalk and afterpulsing
* SensL naming convention: 10000 represents a 1mm detector, 035 a 35μm microcell. Therefore, the 10035 is a 1mm detector with 35μm microcells.
** Vinogradov et al., IEEE Trans. Nucl. Sci., Vol: 58, (2011)
*** Hakim et al., IEEE Trans. Electron Devices, Vol. 37, No.3 (1990)
▲ Measured at room temperature

Source: SensL Sense Light.

ATTACHMENT B – DIFFRACTION GRATING TYPICAL EFFICIENCY

Figure 55 – Diffraction grating typical efficiency – 830 g/mm.

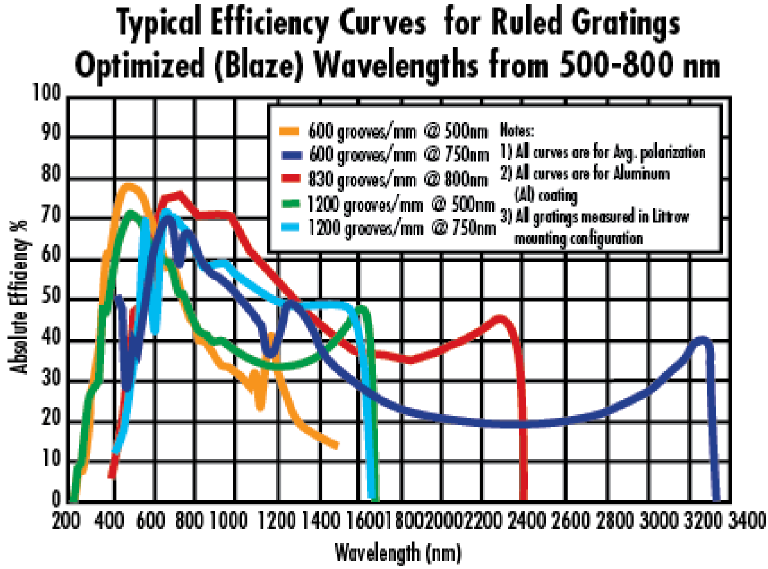

Source: Edmund Optics.